



04572

TECH LIBRARY KAFB, NM

# RESEARCH MEMORANDUM

INVESTIGATION OF INTERFERENCE LIFT, DRAG, AND PITCHING  
MOMENT OF A SERIES OF TRIANGULAR WING AND BODY  
COMBINATIONS AT A MACH NUMBER OF 1.62

By Donald E. Coletti

Langley Aeronautical Laboratory  
Langley Field, Va.

NATIONAL ADVISORY COMMITTEE  
FOR AERONAUTICS

WASHINGTON

May 27, 1955

Classification cancelled (or changed to UNCLASSIFIED)

By Authority: NASA Tech Pub Announcement #125  
(OFFICER AUTHORIZED TO CHANGE)

By ..... 18 Dec 58 .....

..... NMLS .....

GRADE OF OFFICER MAKING CHANGE)

..... 2/11/61 .....

DATE



0143573

Q  
NACA RM L55B25

CONFIDENTIAL

## NATIONAL ADVISORY COMMITTEE FOR AERONAUTICS

## RESEARCH MEMORANDUM

## INVESTIGATION OF INTERFERENCE LIFT, DRAG, AND PITCHING

## MOMENT OF A SERIES OF TRIANGULAR WING AND BODY

## COMBINATIONS AT A MACH NUMBER OF 1.62

By Donald E. Coletti

## SUMMARY

An investigation was made at a Mach number of 1.62 of a series of triangular wing and body combinations to determine the interference lift, drag, and pitching moment.

The models consisted of a series of seven flat-plate triangular wings of varying scale in combination with a body of fineness ratio 10.27. Four wings had half-apex angles of  $30^{\circ}$  while the remaining three had half-apex angles of  $45^{\circ}$ .

The results of the investigation indicated that interference between the wing and body gave an increase in lift over that of a wing and a body alone but at the expense of more drag. Interference also gave reductions in positive pitching moments. The effect of a Reynolds number variation on the lift, drag, and pitching moment of the wing in the presence of the body was generally small. In general, good predictions of the interference lifts and pitching moments on the body due to the wings and on the wings due to the body were obtained by the methods presented in NACA RM A51J04 and NACA RM A52B06 even though some of the predictions for the wing-body combinations and for the wings in the presence of the body were somewhat high.

## INTRODUCTION

In recent years considerable effort has been devoted to the study of the beneficial or detrimental effects of wing-body-tail interference on various aircraft and missile configurations at subsonic, transonic, and supersonic speeds. A compilation of much of the past work relating to this subject can be found in reference 1. More recently, additional work has been presented in reference 2 on the comparison between theoretical and experimental interference pressure fields of a rectangular

HAB 55 25177A

wing and body combination at supersonic speeds. The theoretical analysis had been presented in an earlier report (ref. 3), and comparisons were made of this analysis and other theoretical methods (listed in refs. 1 and 2). The theory of reference 3, in general, agreed well with the experimental results. Additional interference data have also been obtained for a series of rectangular wing and body combinations at supersonic speeds (ref. 4); in this investigation assessments were made of the various theoretical methods for the prediction of interference lift. The results showed that the methods of reference 5 gave satisfactory predictions of the lift of the wing in the presence of the body, the wing due to the body, and the body due to the wing.

The present report is part of a general program in the Langley 9-inch supersonic tunnel to determine the effects of triangular wing plan forms on wing-body interference. The results presented herein were obtained at a Mach number of 1.62, with emphasis upon lift and pitching-moment interference, although drag-interference results are included. The investigation involved a series of seven flat-plate triangular wings of varying size having beveled leading and trailing edges in combination with one standard body of revolution having a fineness ratio of 10.27.

Four of the wings had half-apex angles of  $30^\circ$  with an exposed aspect ratio of 2.3 while the remaining three had half-apex angles of  $45^\circ$  with an exposed aspect ratio of 4.

#### SYMBOLS

$\alpha$	angle of attack of body
$b$	total wing span
$c_r$	wing root chord
$\bar{c}$	mean aerodynamic chord
$C_L$	lift coefficient, Lift/ $qS$
$C_D$	drag coefficient, Drag/ $qS$
$C_m$	pitching-moment coefficient about 50 percent mean aerodynamic chord, Moment/ $qS\bar{c}$
$C_X$	longitudinal-force coefficient for exposed wing in presence of body, $X/qS$

$$C_{L\alpha} = \frac{dC_L}{d\alpha} \text{ at } C_L = 0$$

$$C_{m\alpha} = \frac{dC_m}{d\alpha} \text{ at } C_L = 0$$

$C_{D\min}$  minimum drag coefficient

$C_{L\alpha}'$  lift-curve slope based on maximum body frontal area

$C_{m\alpha}'$  pitching-moment-curve slope based on maximum body frontal area and maximum body diameter

$C_{D\min}'$  minimum drag coefficient based on maximum body frontal area

d body diameter

D maximum body diameter

i angle of wing incidence

L total body length

M Mach number

n fineness ratio,  $L/D$

$l_f$  forebody length from nose to juncture of body and leading edge of wing root chord

$\epsilon$  half-apex angle of wing leading edge

q dynamic pressure,  $\rho V^2/2$

p stream density

R Reynolds number,  $\rho V c / \mu$

S exposed wing area

t maximum wing thickness

v stream velocity

X longitudinal force, positive rearward  
x longitudinal coordinate from nose of body  
 $\mu$  coefficient of viscosity  
A.C. aerodynamic-center position relative to 50 percent mean aerodynamic chord, positive forward

Configuration identification:

B body alone  
W exposed wing alone  
WB wing and body in combination  
W(B) wing in presence of body

Derived measurements:

b(w) interference on body due to wing = WB - [W(B) + B]  
w(b) interference on wing due to body = W(B) - W

#### APPARATUS AND TESTS

##### Tunnel

The Langley 9-inch supersonic tunnel is a closed-throat, single-return, continuous-operating tunnel in which the test section is approximately 9 inches square. Different test Mach numbers are achieved through the use of interchangeable nozzle blocks. Eleven fine-mesh turbulence-damping screens are installed in the settling chamber ahead of the supersonic nozzle. The pressure, temperature, and humidity can be controlled during the tunnel operation.

##### Models

The basic models consisted of a body having a fineness ratio of 10.27 and a series of seven flat-plate triangular wings of varying plan-form scale ratios having beveled leading and trailing edges. Four of the wings had half-apex angles of  $30^\circ$  (exposed aspect ratio of 2.3) while the remaining three had half-apex angles of  $45^\circ$  (exposed aspect ratio of 4). Table I gives the body coordinates and wing-shape parameters. A sketch

of a typical triangular wing mounted on the body is shown in figure 1, and a photograph of all the models including the seven wings tested in the presence of the body, the body, and the two wings tested alone (sting mounted) is shown in figure 2.

An illustration showing how wings in the presence of the body are interchanged is shown in figure 2 of reference 4. However, for some of the wings of this investigation (wings 1, 2, 3, 5, and 6 - see fig. 2), slots had to be cut in the forward and rear center of the wings to fit the body. These slots were cut such that a small gap existed between the wing and body, thereby insuring a free floating wing. The probable effect of the gap will be discussed in more detail in a later section.

#### Balances

A strain-gage balance mounted inside the body was used to obtain the lift, drag, and pitching moment of the wings in the presence of the body. The housing containing this internal balance was closed off at the model and sting bases to prevent any flow of air through the housing at these points. For a detailed description of the balance, see reference 4.

The lift, drag, and pitching moment of the seven triangular wing and body combinations, of the body alone, and of the two wings alone were obtained by an external balance system. The various configurations were sting-mounted to a system of self-balancing beam scales. A detailed description of the installation of the test models and the elimination of the tare forces may also be found in reference 4.

#### Tests

Tests were conducted at a Mach number of 1.62. Measurements were made of lift, drag, and pitching moment about the wing 50 percent mean aerodynamic chord for the wings alone, body alone, wings in the presence of the bodies, and the wing-body combinations. Reynolds numbers of the tests based on the wing mean aerodynamic chord varied from  $0.30 \times 10^6$  to  $2.10 \times 10^6$ . (For a detailed list of Reynolds numbers for the various wings, see table II.) The angle of attack of each configuration was indicated on a scale, graduated in degrees, by means of a light beam reflected from a small mirror mounted flush on the rear of the body and on the sting in the case of the wing alone. The range of angle of attack was approximately  $\pm 6^\circ$ .

Throughout the tests, the dewpoint in the tunnel was maintained at a level where condensation effects would be negligible.

## PRECISION OF DATA

The precision of the various quantities involved in the testing is listed in table II. This extensive table results from the change in the accuracies of the coefficients with wing configuration. It is understandable that for a given uncertainty of a particular quantity, the accuracy of the coefficient derived from this quantity would be a function of the  $S$  and  $\bar{c}$  values. At the lower Reynolds numbers the accuracies of some of the measured quantities (see blanks in table II) were insufficient to obtain reliable interference quantities. This may be attributed to the low loads on the model and its components at the lower Reynolds numbers and to the accuracy of the external balance system at the time of these tests. The present tests were some of the first to utilize the recently installed six-component external balance system; consequently, the improved accuracy now applicable to the system and resulting from modifications to the balance subsequent to the tests of this investigation was lacking. The estimated uncertainties in a given quantity obtained from the strain-gage balance (wing in the presence of the body) were combined by the method which is based on the theory of least squares outlined in reference 6. For the case where the precision varies with the lift, the accuracy was determined at the approximate end of linearity of the lift.

The accuracy of the stream Mach number represents a maximum variation about a mean Mach number throughout the test section.

## PRESENTATION OF DATA

In figures 3 to 18, the aerodynamic characteristics  $C_L$ ,  $C_D$ ,  $C_X$ , and  $C_m$  of the wings alone, body alone, wings and body in combination, and wings in the presence of the body are presented as a function of angle of attack. All the coefficients are based on the exposed wing area of the particular configuration. Since the Reynolds numbers vary both with the wings and with tunnel stagnation pressure, they (Reynolds numbers) are given in the figures.

The results that are presented for the wing in the presence of the body and the wing-body combination were obtained using free floating wings and a gap of approximately 0.003 inch between the wing and body. This gap size is believed to have had negligible effect on the aerodynamic forces; this belief is based on the information presented in reference 7. An examination was made of the gap effect on the various coefficients using wing 1 since it had the longest running gap length of any of the wings. The values obtained for wing 1 from the curves of

reference 7 were of almost the same magnitude as those for a no-gap configuration (from ref. 7, also). Theoretical analysis of reference 7 further shows that viscous effects play a very important part in reducing undesirable gap effects on configurations having very small gaps. Although no experimental evidence is available in the present investigation or in reference 7, it is believed that the boundary layer between wing and body completely encloses the gap to such an extent that any cross-flow effects through the gap would, according to the criteria of reference 7, be negligible.

#### DISCUSSION OF RESULTS

##### Wing Alone, General

Lift-curve slopes, pitching-moment-curve slopes, and minimum drags of the wings alone were obtained by testing one wing from each group of wings having half-apex angles of  $30^\circ$  and  $45^\circ$ . These two wings were tested over a range of Reynolds numbers equivalent to that which would be obtained if wings 1 to 7 were tested. Wings 2 and 6 were selected since their scale factors were such that equivalent Reynolds numbers could easily be obtained within the limits of the tunnel operation. The Reynolds numbers were obtained by varying the tunnel stagnation pressure. It is realized that the thickness ratios of wings 2 and 6 (wing alone, table I) do not correspond to all of the thickness ratios of wings from 1 to 7 (see table I). Therefore, some of the minimum drags cannot be compared directly even for equivalent Reynolds numbers. Corrective measures were not made to the data with regard to the thickness-ratio effect; discussions concerning this will be presented in later sections. The lift, drag, and pitching-moment coefficients of wings 2 and 6 are presented in figures 17 and 18, respectively, as functions of angle of attack for various values of Reynolds numbers. Lift-curve slopes, pitching-moment-curve slopes, and minimum drags are shown in figure 19 for wings 2 and 6. The coefficients corresponding to the Reynolds numbers of wings 1 to 7 obtained from the faired curves of figure 19 are tabulated in table III.

##### Wing in the Presence of the Body,

##### Reynolds Number Effect

The effect of Reynolds number on the aerodynamic characteristics for the wings in the presence of the body is shown in figure 20. It is seen that, for the configurations investigated, the lift increases with increasing Reynolds number for any one wing. This small increase in lift is probably due to a decrease in separation at the wing trailing edge and body juncture in going from a low to a high Reynolds number. It is further seen that as the Reynolds number is increased, the pitching moment decreases slightly for any one wing. This could also indicate a decreasing region of separation with increasing Reynolds number, and in turn cause a slight rearward shift of the aerodynamic center. It is, of course, realized that this slight decrease of pitching moment may not be too significant (particularly for  $\epsilon = 30^\circ$ ) since for some wings this decrease is of the order of the accuracy of the measurements.

Figure 20 also shows a small increase in drag for any one wing due to increasing Reynolds number for most of the wings in the presence of the body. This increase in drag is apparently due to an increase in skin friction since the Reynolds numbers of these wings are probably in the transitional region between the laminar and turbulent boundary layer. It is further seen from figure 20, that the smaller wings generally have higher drag coefficients than the larger wings. This is, at least in part, due to the increase in wave drag that results from increasing thickness ratio with decreasing wing size (see table I and figure 2). A substantiation of this was made by using an approximation involving ratios of  $(t/c^2)$  for the wings.

#### Basic Quantities for Interference Evaluation

Figures 21 and 22 show, for configurations involving wings having  $\epsilon = 30^\circ$  and  $\epsilon = 45^\circ$ , respectively, the variation of lift-curve slope, pitching-moment-curve slope, and minimum drag values with ratios of  $b/D$  for the wing and body in combination WB, wing in the presence of the body W(B), body alone B, and the wing alone W. In these same figures, comparisons are made between experiment and theory of some of the configurations and coefficients. The experimental quantities are taken directly from the curves in figures 3 to 19. The coefficients of the wings and body alone are based on the exposed wing area and are presented as functions of  $b/D$  for consistency purposes and for the convenience of comparison with the remaining configurations.

W.- The theoretical lifts for the wings alone were obtained from reference 8. Brown's theory was used for the subsonic-leading-edge wing ( $\epsilon = 30^\circ$  shown in fig. 21) and Ackeret's result was used for the supersonic-leading-edge wing ( $\epsilon = 45^\circ$  shown in fig. 22). The theoretical values, while somewhat higher than those obtained experimentally, are, nevertheless, in fair agreement with the experimental values.

Since linear theory predicts the center of pressure at the centroid of the area or 50 percent mean aerodynamic chord, the theoretical pitching moment is zero for this investigation.

B.- The theoretical lifts and pitching moments for the body alone were obtained from the theory presented in reference 9. As seen from the figures, this theory agrees satisfactorily with the experimental results.

W(B).- The methods for predicting the lifts and pitching moments of the wings in the presence of the body are found in references 5 and 10. As seen from figures 21 and 22, the agreement of the methods with the experimental results is fair for the lifts and good for the pitching moments. Since the method for obtaining the force on the wing in the presence of the body is calculated as a percentage of the force on the

wing alone, better agreement could be expected if the predictions of the wing-alone forces were improved. In engineering applications if experimental wing-alone results were available these should be used in determining the forces and moments of the wing in the presence of the body.

The minimum drag coefficients for all the wings in the presence of the body, shown in figures 21 and 22, do not take into account the effects due to the different thickness ratio. If these effects were considered, it is probable that the trend of drags would parallel that for the wings alone in going from a low to a high  $b/D$ . It is obvious then that the interference drag on the wing due to the body would also be affected.

WB.- The comparisons between the experimental lifts and pitching moments for the wing-body combinations and the methods presented in references 5 and 10 are in better agreement than are similar comparisons for the wings in the presence of the body. As seen in figures 21 and 22 the differences between the experimental and the predicted lifts for the wings in the presence of the body are slightly larger than are those for the wing and body combinations. The calculated forces and moments for the wing-body combinations were obtained in the same manner as were those for the wings in the presence of the body, namely, a percentage of the forces on the wing alone.

#### Interference Quantities

General.- The interference on the body due to the wing is obtained by subtracting the forces on the wing in the presence of the body and body alone from that of the wing-body combination; that is,

$b(w) = WB - [W(B) + B]$ . In like manner, the interference on the wing due to the body is the difference between the forces on the wing in the presence of the body and on the wing alone in free stream; that is,  
 $w(b) = W(B) - W$ .

A summation of the interference quantities for the body due to the wing  $b(w)$  and the wing due to the body  $w(b)$  is presented as a function of  $b/D$  in figure 23 and  $c_r/D$  in figure 24 for the series of the wing and body combinations. In figures 23(a) and 23(b), the values are based on the exposed wing area since the methods of references 5 and 10 for the predictions of the interference quantities base the coefficients on the area of the exposed wing. In figures 23(c) and 23(d) and figures 24(a) and 24(b), the values are based on the maximum body frontal area and maximum body diameter. If differences between the interference forces on the body due to the wing are to be explained for the various wing-body combinations, it is understandable that erroneous conclusions could be made concerning some of the quantities with the coefficients based on the exposed wing area. For this reason, discussions concerning the effects

between the various wing-body combinations will be confined to coefficients based on maximum body frontal area and maximum body diameter for the case of the body due to the wing and on exposed wing area for the case of the wing due to the body.

Lift,  $b(w)$ . - A comparison between the experimental lift on the body due to the wing with the theoretical method is shown in figure 23(a). The agreement is good considering that the prediction of the absolute values for the  $W$ ,  $W(B)$ , and  $WB$  were somewhat high. As seen from this figure, the lift decreases with increasing  $b/D$  or exposed wing area; however, when the values are based on a common area (see figs. 23(c) and 24(a)), the interference lift increases with increasing wing size as would be expected. From figure 25, the interference lift on the body due to the wing is seen to be predominately that which carries over from the wing to the body between the Mach helices emanating from the leading- and trailing-edge root-chord junction. Figure 25 also indicates that with decreasing wing scale, the area upon which this interference lift acts decreases, resulting in less interference lift. From figure 24(a), the lift on the body due to the wing for any given  $c_r/D$  is less for configurations with wings having  $\epsilon = 30^\circ$  than for those having  $\epsilon = 45^\circ$ . This is apparently due to the fact that the higher lift for the supersonic-leading-edge wing (as compared with that for the subsonic-leading-edge wing) carries over onto the body.

In addition to this positive carryover lift, an induced negative lift, created by the vortex action of the wing, acts on the afterbody. Since there were no definite results in the present investigation pointing to this induced negative lift, it is probable that this lift represents a small percentage of the total interference. This was also found to be the condition that existed for the rectangular wings in reference 4.

It is of interest to point out the divergence of the lifts in figure 24(a) for configurations with wings having  $\epsilon = 30^\circ$  and  $45^\circ$  in going from a high to a low  $c_r/D$ . The exact cause of this divergence is unknown; however, it might be due to vorticity effects and upwash effects on the wings from the noncylindrical portions of the body.

Pitching moment,  $b(w)$ . - Figure 23(a) shows that the agreement between the experimental and theoretical pitching moment for the body due to the wing is good at the high values of  $b/D$  but poor at the low values of  $b/D$ . Some of this poor agreement at the low values of  $b/D$  may be due to the low accuracy of the experimental measurements for the smaller wings. (See, for example, wing 4 in table II.)

With reference to the sketches in figure 25, the wing-root lift carryover onto the body acts behind the center of gravity so that a negative pitching moment is obtained. This is shown experimentally in

figures 23 and 24. It is further seen that more negative pitching moment is obtained with decreasing wing size with the exception of the two smallest wings. In these cases, the moments become less negative than that established by the trends of the other wings. This is because the coefficients are based on the maximum body diameter which is larger than the mean aerodynamic chords of the two wings.

Aerodynamic center,  $b(w)$ . - As seen in figure 23(a), the theoretical aerodynamic centers are in good agreement with the experimental results at high values of  $b/D$  and in poor agreement at low values of  $b/D$ . The variation of the aerodynamic centers with  $b/D$  shows that for configurations having  $\epsilon = 45^\circ$  wings, the interference lift center is farther rearward along the body than for  $\epsilon = 30^\circ$  configurations. If the aerodynamic centers were shown as functions of  $c_r/D$  values, the reverse would be true.

Drag,  $b(w)$ . - When the coefficients are based on the exposed wing area the variation of the interference drag on the body due to the wing decreases with increasing  $b/D$  as shown in figure 23(a). However, when the coefficients are based on the maximum body frontal area, the variation with  $b/D$  or  $c_r/D$  (figs. 23(c) and 24(a)) is very nearly constant. This again indicates why care should be taken in deciding upon what areas the coefficients are to be based since erroneous conclusions could result. An approximation was made of the skin friction on the body with and without a wing by the procedure used in reference 4. First, it was assumed that the boundary layer was laminar on the body alone at the Reynolds number of this investigation. Also, it was assumed that the wave drag was constant regardless of the type of boundary layer, and that for the wing-body combination the boundary layer changed from laminar to turbulent on the body at the intersection of the Mach helices emanating from the leading-edge root-chord junctures. The results of this approximation for the increase in body drag due to increase in skin friction indicated that the interference effects of the wing upon the minimum body drag are predominately skin-friction effects.

Lift,  $w(b)$ . - Figure 23(b) shows that good agreement is obtained between the experimental lift on the wing due to the body and theory even though the prediction of the absolute values for the  $W$  and  $W(B)$  were somewhat high. With the coefficients based on the exposed wing area (fig. 23(b)), it is seen that higher lift coefficients are obtained on the smaller wings. In all probability this is due to the fact that more of the area of the smaller wings is in the stronger upwash field of the body compared with that for the larger wings. It is further seen that, for any given  $b/D$ , the interference lift coefficient is greater for the  $\epsilon = 45^\circ$  configuration than for the  $\epsilon = 30^\circ$  case. Of course, when the coefficients are based on the maximum body frontal area (figs. 23(d) and 24(b)), more positive lift coefficients are obtained from the larger wings.

~~CONFIDENTIAL~~

Pitching moment, w(b). - With consideration of the accuracy, the interference pitching moment of the wing due to the body, for all practical purposes, is negligible for configurations involving wings 3, 4, 6, and 7 as shown by figures 23(b), 23(d), and 24(b). For configurations involving wings 1, 2, and 5 a small negative moment is obtained. The causes and effects of these small negative moments will be discussed in more detail in the section dealing with the percentage contributions of the basic and interference quantities to the complete configuration.

Aerodynamic center, w(b). - The interference aerodynamic centers shown in figure 23(b) follow the same trends as the pitching moments. The location of the interference aerodynamic centers may be explained by the conditions that for wings 1, 2, and 5 the interference lift center is slightly rearward of the centroid of the wing areas (resulting in a negative pitching moment), whereas for wings 3, 4, 6, and 7 the interference lift center is very nearly coincident with the centroid of the wing areas or the 50 percent mean aerodynamic chord.

Drag, w(b). - The interference drags on the wings due to the body are shown in figures 23(b), 23(d), and 24(b). However, as was mentioned previously, the effect of wing thickness ratio (which was not taken into account in the analysis) would alter the variation of these drags. From estimations made to account for this thickness-ratio effect, the interference drags of figure 23(b) would be changed to give a more positive slope in going from low to high values of  $b/D$ . In any case, most of the drag is apparently due to skin-friction effects.

#### Contributions of the Basic and Interference Quantities

In order to assess the relative effects of each quantity on the complete configuration, each of the basic and interference quantities of lift, pitching moment, and drag are shown in figure 26 as a function of the total lift, pitching moment, and drag of the complete configuration. Figure 26(a) presents the fractional breakdown of the various elements for the configurations involving the wings of  $\epsilon = 30^\circ$ ; whereas figure 26(b), the configurations involving the wings of  $\epsilon = 45^\circ$ . It is seen from this figure that the interference lift on the  $w(b)$  and  $b(w)$  is very beneficial for the configurations involving wings of  $\epsilon = 30^\circ$  or  $45^\circ$ . Between a 21-percent and 38-percent increase in lift can be realized, because of interference, over that which could be obtained by simply adding the lifts of the wing alone and the body alone. It is further seen, that within a few percent, the percentage interference lift contribution on the  $b(w)$  and  $w(b)$  for the  $\epsilon = 30^\circ$  and  $45^\circ$  configurations is very nearly constant.

The pitching-moment contribution of the various lift quantities for all the wing-body combinations illustrates clearly that the lift on the  $b(w)$  acts behind the centroid of the wing areas and that the moment

~~CONFIDENTIAL~~

is generally more negative with decreasing ratios of  $b/D$ . Between a 13-percent and a 33-percent reduction in positive pitching moment is realized because of interference over that which could be obtained by summing the pitching moments of the wing alone and of the body alone. Both the wing alone and wing in the presence of the body contribute a positive moment, showing that the aerodynamic center is ahead of the centroid of the wing area. The body moment contribution is by far the largest positive moment since its aerodynamic center is in the region of the nose of the body. As was mentioned earlier in connection with figure 23(b), negative interference moments on the  $w(b)$  were obtained from configurations involving wings 1, 2, and 5 with  $b/D$  ratios of 5.60, 4.58, and 7.41, respectively (also shown in fig. 26). As seen from figure 25, there appears to be an association of these negative interference moments with the Mach lines emanating from the junctures of the wing leading edge and the body in that when these Mach lines cross the wing trailing edges these negative interference moments occur. For all practical purposes, no interference moments occur when these Mach lines do not cross the trailing edges. A possible explanation of the negative interference moments may lie in the interference lifting pressures at the juncture of the wing leading edge and the body carrying over the body along the ray (or Mach line in fig. 25) and crossing the wing trailing edge. This would result in a region of higher lifting pressures than would occur for the wing alone.

The fractional breakdown of the various drag quantities is somewhat as would be expected. That is, the low  $b/D$  wings alone contribute a smaller percentage of drag to the total than do the large  $b/D$  wings alone; whereas, the drag contribution of the body is the reverse. The drags for the  $w(b)$  are presented as obtained from the tests with no corrections due to thickness ratio.

#### CONCLUSIONS

An investigation was made of the interference effects on a series of seven flat-plate triangular wings of varying scale in combination with a body having a fineness ratio of 10.27. Four of the wings had half-apex angles of  $30^\circ$  while the remaining three had half-apex angles of  $45^\circ$ . Basic measurements of lift, drag, and pitching moment were obtained for the wing-body combinations, wing in presence of the body, wing alone, and body alone at a Mach number of 1.62. Interference lifts, drags, and pitching moments were obtained from the basic measurements. The results indicate that:

1. Interference gave between a 21-percent and 38-percent increase in lift over that which would be obtained by summing the lifts of the

wing alone and of the body alone. This was accompanied by an increase in drag due to skin friction. For some configurations, a negative interference moment was obtained on the wing due to the body.

2. The method presented in NACA RM A51J04 gave good predictions of the interference lifts on the body due to the wing and on the wing due to the body for all configurations even though the lift predictions for the wing-body combinations and for the wings in the presence of the body were somewhat high.

3. Interference gave between a 13-percent and a 33-percent reduction in positive pitching moment from that which would be obtained by summing the pitching moments of the wing alone and of the body alone.

4. The prediction of the interference pitching moments on the body due to the wings using the method in NACA RM A52B06 was in good agreement at the higher ratios of wing span to body diameter  $b/D$  and poor at the low  $b/D$  ratios. The experimental pitching moments of the wing in the presence of the body and wing-body combinations were also in good agreement with the above method.

5. The theoretical lift and pitching moment of the body alone presented in NACA RM A50L07 agreed well with the experimental results.

6. Only fair agreement was obtained between the experimental lift of the wings alone and that predicted by linear theory. Since the theoretical lifts of the wings in the presence of the body and the wing-body combinations are functions of the wing-alone values, it is understandable that the agreement between experiment and theory for these two basic quantities is also only fair.

7. Within the limits of this investigation, the effect of varying Reynolds number upon the lifts, drags, and pitching moments for the wings in the presence of the body was generally small.

8. The interference drags on the body due to the wings were a large percentage of the total wing-body drags, whereas the interference drags on the wings due to the body were relatively small percentages of the total drags. These interference drags were probably due to changes in skin-friction drags.

Langley Aeronautical Laboratory,  
National Advisory Committee for Aeronautics,  
Langley Field, Va., February 15, 1955.

## REFERENCES

1. Nielsen, Jack N., Kaattari, George E., and Anastasio, Robert F.: A Method for Calculating the Lift and Center of Pressure of Wing-Body-Tail Combinations at Subsonic, Transonic, and Supersonic Speeds. NACA RM A53G08, 1953.
2. Pitts, William C., Nielsen, Jack N., and Gionfriddo, Maurice P.: Comparison Between Theory and Experiment for Interference Pressure Field Between Wing and Body at Supersonic Speeds. NACA TN 3128, 1954.
3. Nielsen, Jack N., and Pitts, William C.: Wing-Body Interference at Supersonic Speeds With an Application to Combinations With Rectangular Wings. NACA TN 2677, 1952.
4. Coletti, Donald E.: Investigation of Interference Lift, Drag, and Pitching Moment of a Series of Rectangular Wing and Body Combinations at Mach Numbers of 1.62, 1.93, and 2.41. NACA RM L52E26, 1952.
5. Nielsen, Jack N., and Kaattari, George E.: Method for Estimating Lift Interference of Wing-Body Combinations at Supersonic Speeds. NACA RM A51J04, 1951.
6. Michels, Walter C.: Advanced Electrical Measurements. Second ed., D. Van Nostrand Co., Inc., 1941.
7. Bleviss, Z. O., and Struble, R. A.: Some Aerodynamic Effects of Streamwise Gaps in Low Aspect Ratio Lifting Surfaces at Supersonic Speeds. Jour. Aero. Sci., vol. 21, no. 10, Oct. 1954. pp. 665-674, 680.
8. Brown, Clinton E.: Theoretical Lift and Drag of Thin Triangular Wings at Supersonic Speeds. NACA Rep. No. 839, 1946. (Supersedes NACA TN 1183.)
9. Allen, H. Julian, and Perkins, Edward W.: Characteristics of Flow Over Inclined Bodies of Revolution. NACA RM A50L07, 1951.
10. Kaattari, George E., Nielsen, Jack N., and Pitts, William C.: Method for Estimating Pitching-Moment Interference of Wing-Body Combinations at Supersonic Speed. NACA RM A52B06, 1952.

TABLE I

## BODY COORDINATES AND WING-SHAPE PARAMETERS

[See fig. 1.]

Body	
x, in.	Diameter, in.
0	0.002
.500	.154
1.000	.296
1.500	.430
2.000	.552
2.500	.660
3.000	.746
3.500	.820
3.750	.846
4.000	.860
4.625	.872
5.000	.876
5.500	.874
6.000	.872
6.500	.866
7.250	.794
8.000	.692
8.375	.628
9.000	.500

Type	Flat-plate triangular wings											
	Designation	$\epsilon$ , deg	b/D	c <sub>r</sub> /D	S, sq in.	c <sub>r</sub> , in.	b, in.	$\bar{c}$ , in.	i, deg	t, in.	$t^*$ , in.	t/ $\bar{c}$
Wing in presence of body	1	30	5.60	4.148	7.131	3.634	4.914	2.423	0.24	0.049	2.850	0.0202
	2	30	4.58	3.190	4.311	2.795	4.022	1.863	.01	.040	3.457	.0215
	3	30	3.62	2.257	2.274	1.977	3.179	1.318	-.12	.031	4.273	.0235
	4	30	2.63	1.424	.900	1.248	2.312	.832	-.55	.020	4.685	.0240
	5	45	7.41	3.213	7.947	2.815	6.497	1.876	-.01	.051	3.691	.0272
	6	45	5.69	2.338	4.209	2.048	4.991	1.365	-.06	.042	4.203	.0308
	7	45	3.62	1.325	1.340	1.161	3.177	.774	-.15	.027	4.779	.0349
Wing alone	2	30	----	----	4.281	2.789	3.070	1.859	----	.041	----	.0221
	6	45	----	----	4.142	2.043	4.055	1.362	----	.042	----	.0308

TABLE II

## SUMMARY OF TOTAL UNCERTAINTIES

Wing configuration	R	Accuracy at $C_L = 0$ for WB, B, W			Accuracy at $C_L = 0$ for W(B)			Accuracy at approximate end of linearity for W(B)		Inaccuracy of slopes for WB, B, W		Inaccuracy of slopes for W(B)		Inaccuracies for b(w)			Inaccuracies for w(b)				
		$C_L$	$C_m$	$C_D$	$C_L$	$C_m$	$C_D$	$C_{L_w}$	$C_{m_w}$	$C_{T_w}$	$C_{m_w}$	$C_{T_w}$	$C_{m_w}$	$ C_{D_{min}} $	$C_{L_w}$	$C_{m_w}$	$C_{D_{min}}$				
1	$0.95 \times 10^6$ 2.10	$\pm 0.0001$	$\pm 0.0007$	$\pm 0.0001$	$\pm 0.0004$	$\pm 0.0001$	$\pm 0.0001$	$\pm 0.0006$	$\pm 0.0002$	$\pm 0.0001$	$\pm 0.0002$	$\pm 0.0001$	$\pm 0.0001$	$\pm 0.0003$	$\pm 0.0001$	$\pm 0.0002$	$\pm 0.0005$	$\pm 0.0002$	$\pm 0.0001$	$\pm 0.0004$	$\pm 0.0001$
2	.71 1.62	$\pm 0.0002$	$\pm 0.0010$	$\pm 0.0001$	$\pm 0.0007$	$\pm 0.0003$	$\pm 0.0002$	$\pm 0.0010$	$\pm 0.0003$	$\pm 0.0001$	$\pm 0.0002$	$\pm 0.0001$	$\pm 0.0005$	$\pm 0.0002$	$\pm 0.0001$	$\pm 0.0002$	$\pm 0.0007$	$\pm 0.0002$	$\pm 0.0005$	$\pm 0.0001$	
3	.50 1.46	$\pm 0.0003$	$\pm 0.0020$	$\pm 0.0002$	$\pm 0.0013$	$\pm 0.0009$	$\pm 0.0004$	$\pm 0.0019$	$\pm 0.0013$	$\pm 0.0001$	$\pm 0.0010$	$\pm 0.0003$	$\pm 0.0009$	$\pm 0.0006$	$\pm 0.0003$	$\pm 0.0002$	$\pm 0.0003$	$\pm 0.0005$	$\pm 0.0005$	$\pm 0.0002$	
4	.30 .92	$\pm 0.0008$	$\pm 0.0002$	$\pm 0.0005$	$\pm 0.0034$	$\pm 0.0036$	$\pm 0.0012$	$\pm 0.0050$	$\pm 0.0055$	$\pm 0.0004$	$\pm 0.0041$	$\pm 0.0006$	$\pm 0.0025$	$\pm 0.0027$	$\pm 0.0010$	$\pm 0.0058$	$\pm 0.0006$	$\pm 0.0008$	$\pm 0.0011$	$\pm 0.0005$	
5	.71 1.61	$\pm 0.0001$	$\pm 0.0005$	$\pm 0.0001$	$\pm 0.0004$	$\pm 0.0002$	$\pm 0.0001$	$\pm 0.0005$	$\pm 0.0003$	$\pm 0.0001$	$\pm 0.0002$	$\pm 0.0001$	$\pm 0.0002$	$\pm 0.0001$	$\pm 0.0001$	$\pm 0.0002$	$\pm 0.0003$	$\pm 0.0002$	$\pm 0.0001$	$\pm 0.0005$	$\pm 0.0001$
6	.50 1.17	$\pm 0.0002$	$\pm 0.0014$	$\pm 0.0001$	$\pm 0.0007$	$\pm 0.0005$	$\pm 0.0002$	$\pm 0.0010$	$\pm 0.0007$	$\pm 0.0001$	$\pm 0.0007$	$\pm 0.0002$	$\pm 0.0005$	$\pm 0.0003$	$\pm 0.0002$	$\pm 0.0010$	$\pm 0.0002$	$\pm 0.0002$	$\pm 0.0007$	$\pm 0.0001$	
7	.30 .68	$\pm 0.0007$	$\pm 0.0079$	$\pm 0.0005$	$\pm 0.0022$	$\pm 0.0025$	$\pm 0.0008$	$\pm 0.0032$	$\pm 0.0039$	$\pm 0.0003$	$\pm 0.0059$	$\pm 0.0007$	$\pm 0.0016$	$\pm 0.0019$	$\pm 0.0003$	$\pm 0.0008$	$\pm 0.0055$	$\pm 0.0005$	$\pm 0.0007$	$\pm 0.0012$	$\pm 0.0004$

Configuration	Initial angle of attack	Relative angle of attack	Incidence angle of wings	Mach number	Reynolds number per inch	Stream pressure
All	$\pm 0.05^\circ$	$\pm 0.01^\circ$	$\pm 0.05^\circ$	4.01	±12,000	±1.5 percent

TABLE III

SUMMARY OF LIFT-CURVE AND PITCHING-MOMENT-CURVE SLOPES, AND MINIMUM  
DRAG VALUES AT ZERO LIFT FROM FIGURES 3 TO 19

Wing	R	Wing-body combination, WB			Wing in presence of body, W(B)			Wing, W (a)			Body, B		
		$C_{L_\alpha}$	$C_{m_\alpha}$	$C_{D_{min}}$	$C_{L_\alpha}$	$C_{m_\alpha}$	$C_{D_{min}}$	$C_{L_\alpha}$	$C_{m_\alpha}$	$C_{D_{min}}$	$C_{L_\alpha}$	$C_{m_\alpha}$	$C_{D_{min}}$
1	$0.95 \times 10^6$ 2.10	0.0578	0.0054	0.0205	0.0441 .0467	0.0009 .0008	0.0079 .0089	0.0406	0.0017	0.0085	0.0016	0.0055	0.0063
2	.71 1.62	.0617	.0103	.0257	.0439 .0469	.0013 .0010	.0078 .0086	.0403	.0018	.0071	.0027	.0120	.0105
3	.50 1.46	.0701	.0290	.0480	.0475 .0492	.0020 .0020	.0090 .0103	.0402	.0020	.0067	.0051	.0353	.0228
4	.30 .92	.0852	.1159	.1050	.0521 .0540	.0039 .0032	.0090 .0110	.0393	.0025	.0052	.0129	.1398	.0576
5	.71 1.61	.0624	.0081	.0212	.0501 .0538	.0032 .0018	.0115 .0126	.0483	.0028	.0130	.0015	.0066	.0056
6	.50 1.17	.0693	.0179	.0340	.0524 .0563	.0041 .0027	.0126 .0144	.0482	.0025	.0122	.0029	.0180	.0109
7	.30 .68	.0877	.0836	.0620	.0566 .0602	.0034 .0023	.0162 .0155	.0470	.0030	.0106	.0089	.0963	.0330

<sup>a</sup>Data obtained at equivalent Reynolds numbers.

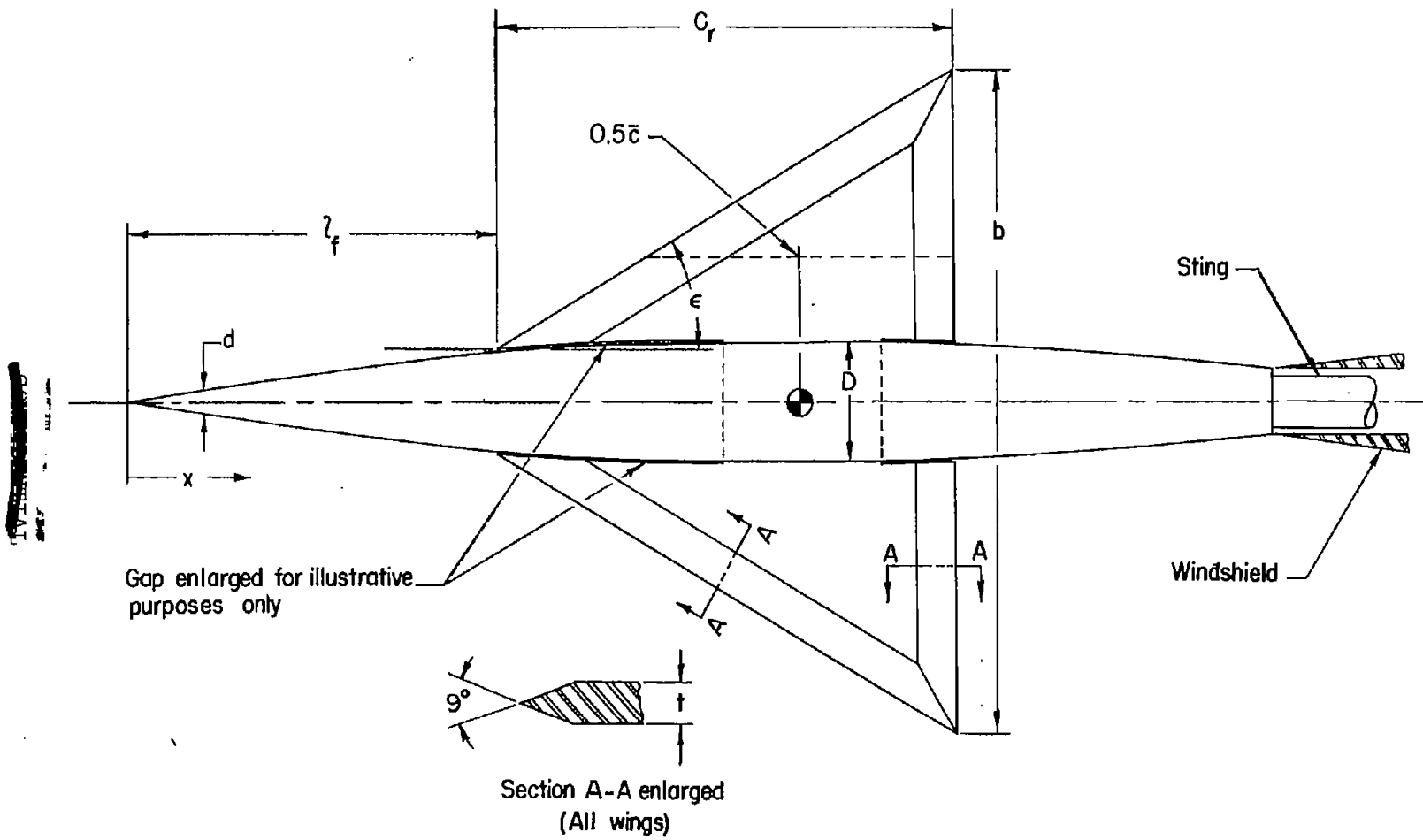


Figure 1.-- Sketch of a triangular wing mounted on an  $n = 10.27$  body.  
Body coordinates and wing-shape parameters are listed in table I.

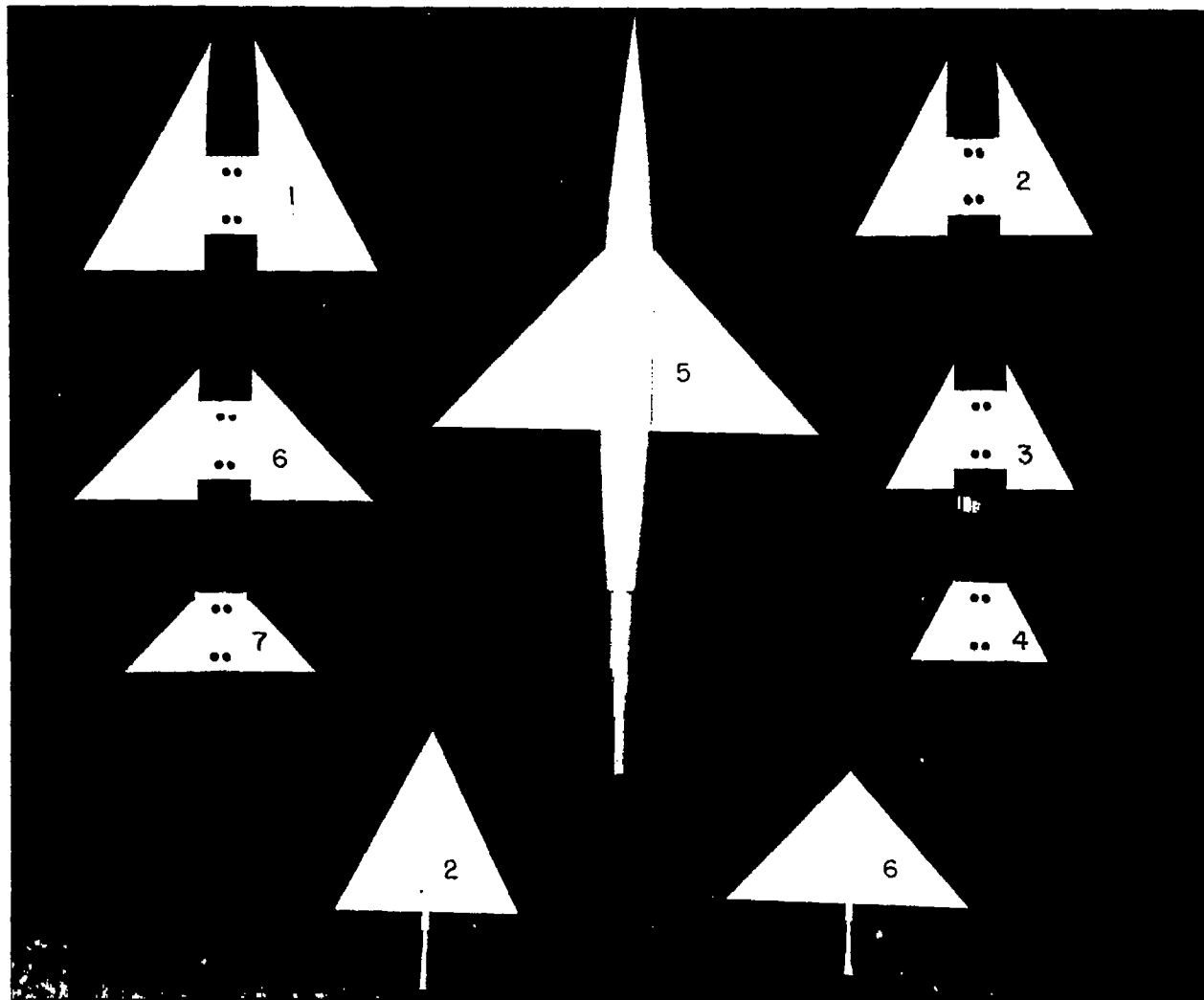


Figure 2.- Photograph of the models tested.

I-87905

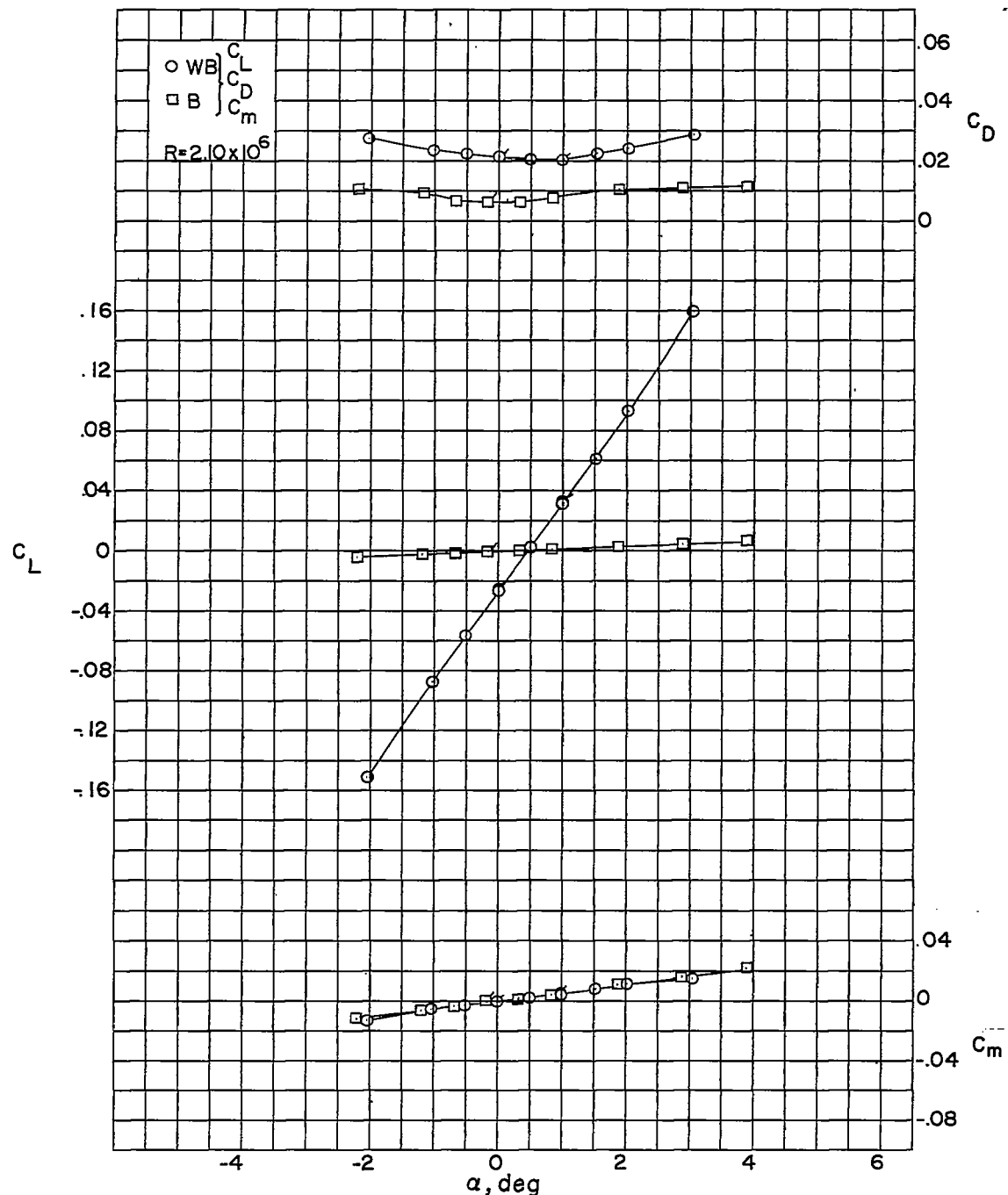


Figure 3.- Aerodynamic characteristics of the wing and body combination for triangular wing 1 ( $\epsilon = 30^\circ$ ) and the body alone. (Body-alone results are based on exposed area of triangular wing 1.) Flagged symbols denote check values.

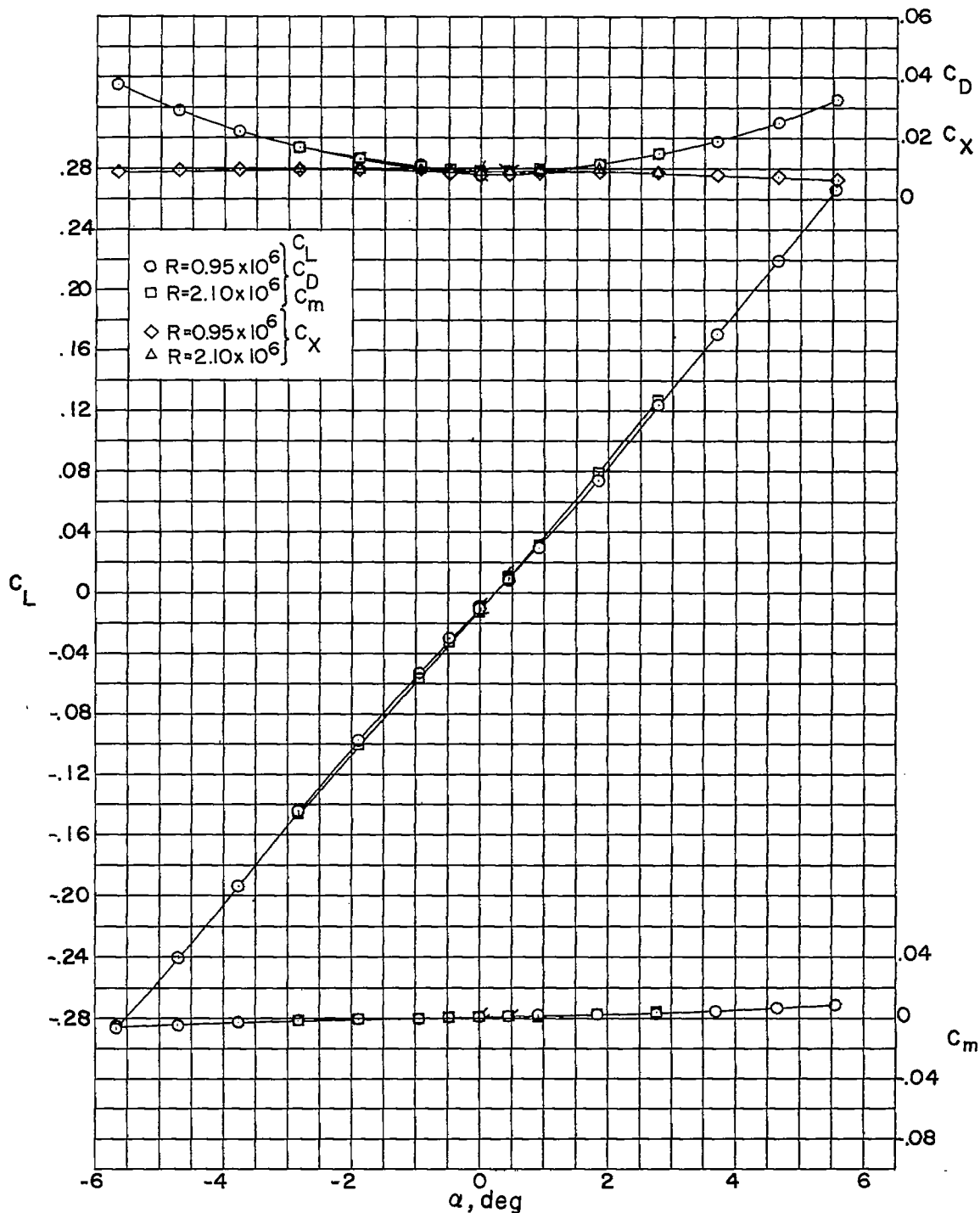


Figure 4.- Aerodynamic characteristics of the wing in the presence of the body for triangular wing 1 ( $\epsilon = 30^\circ$ ). Flagged symbols denote check values.

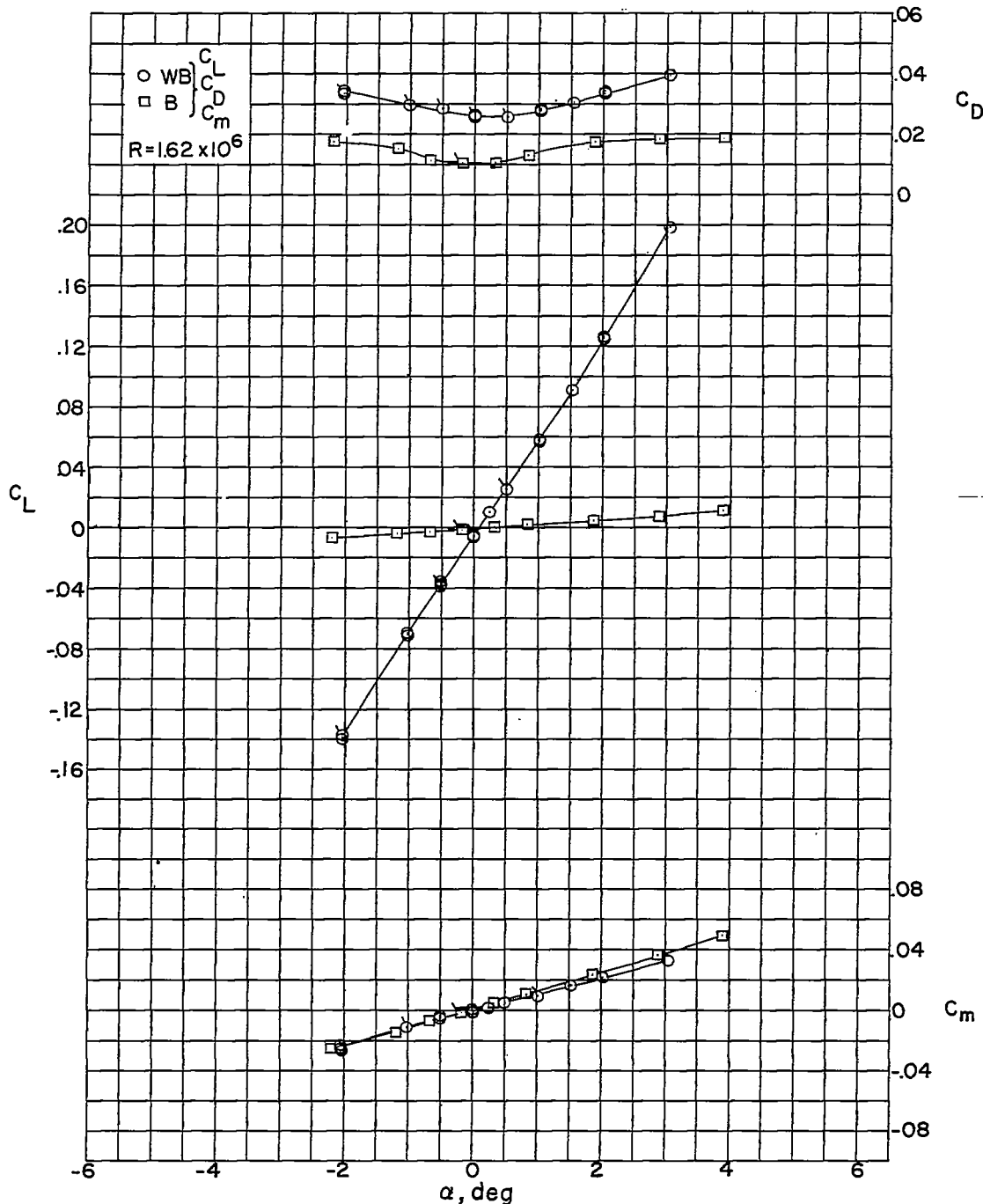


Figure 5.- Aerodynamic characteristics of the wing and body combination for triangular wing 2 ( $\epsilon = 30^\circ$ ) and the body alone. Body-alone results are based on exposed area of triangular wing 2.) Flagged symbols denote check values.

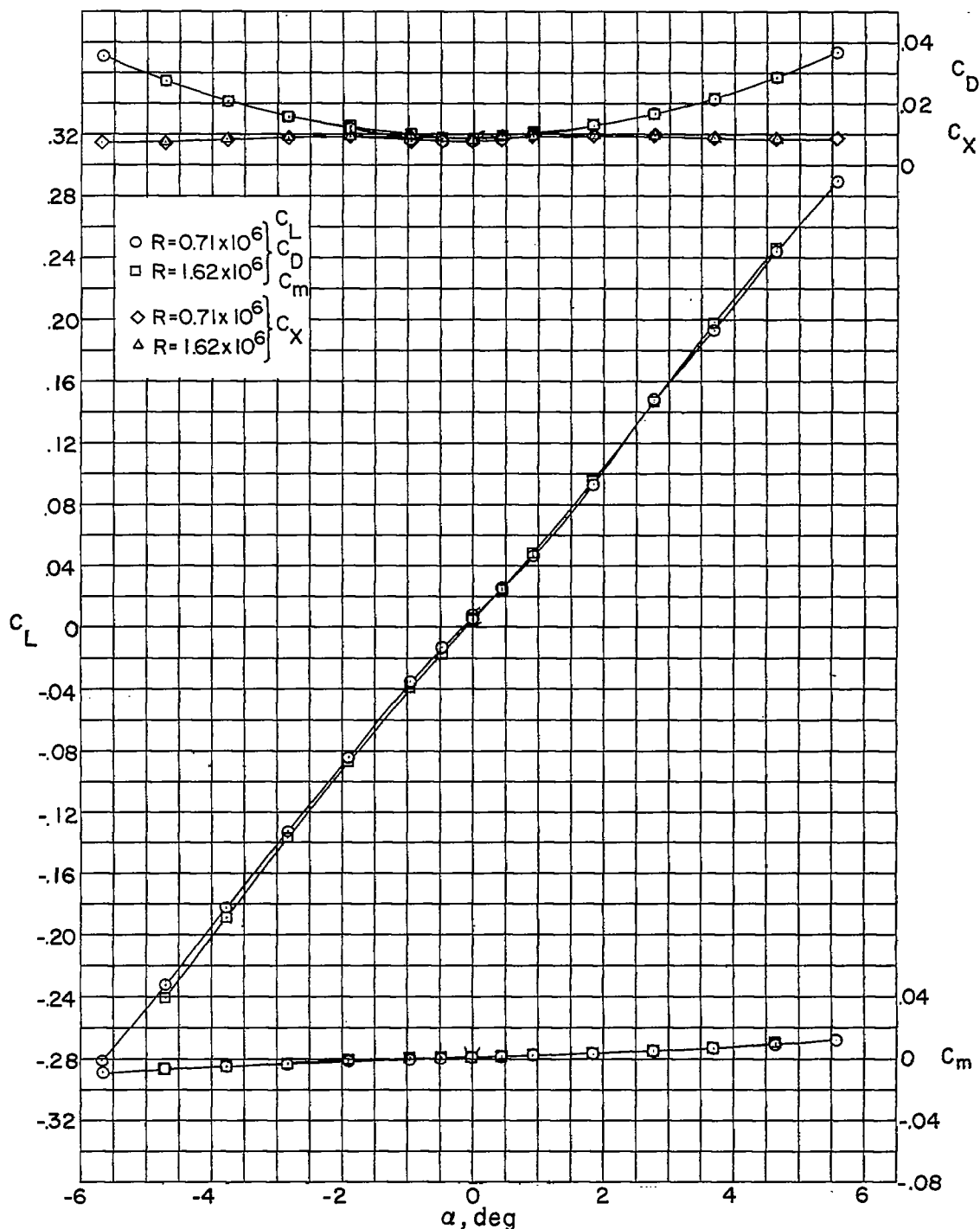


Figure 6.- Aerodynamic characteristics of the wing in the presence of the body for triangular wing 2 ( $\epsilon = 30^\circ$ ). Flagged symbols denote check values.

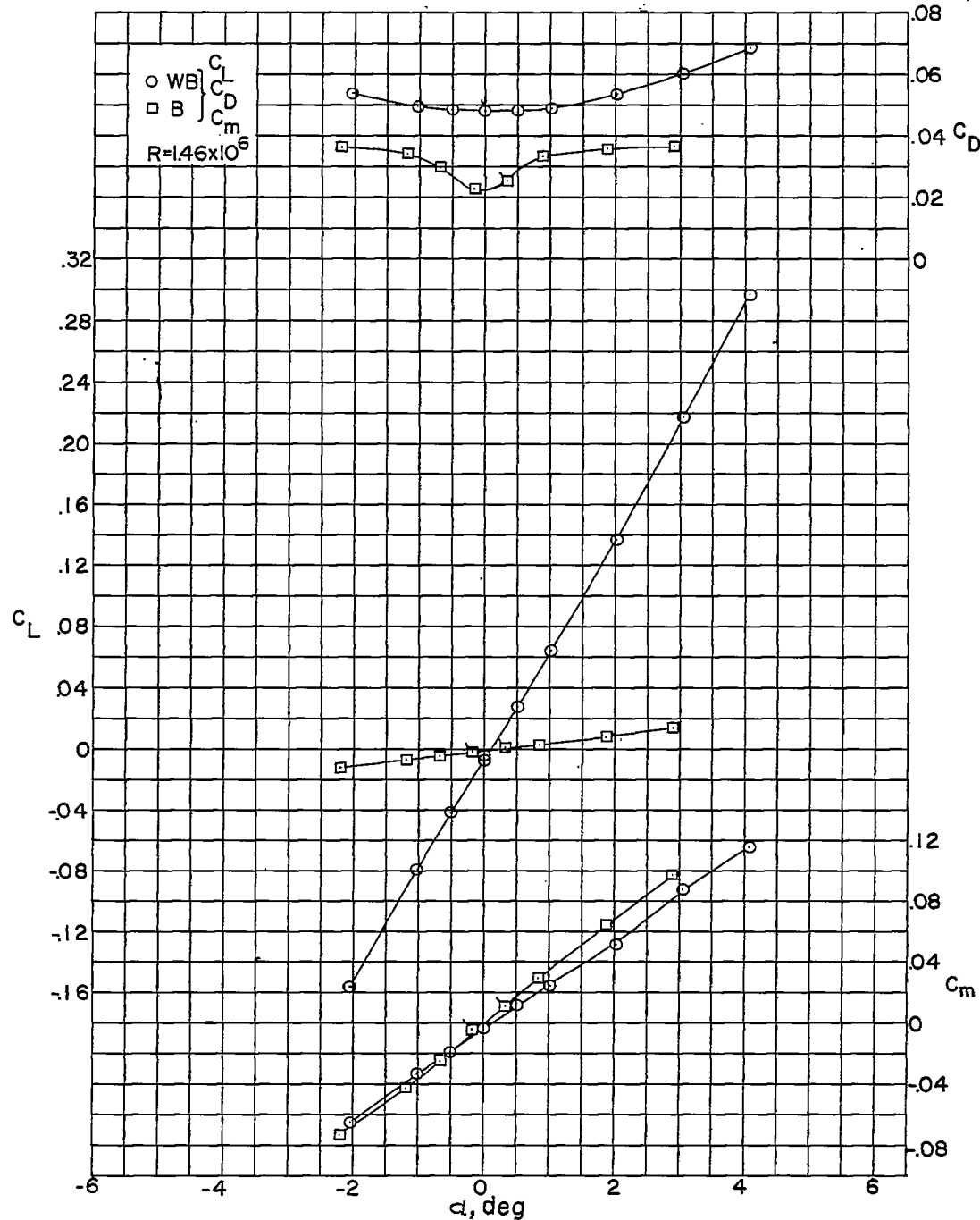


Figure 7.- Aerodynamic characteristics of the wing and body combination for triangular wing 3 ( $\epsilon = 30^\circ$ ) and the body alone. (Body-alone results are based on exposed area of triangular wing 3.) Flagged symbols denote check values.

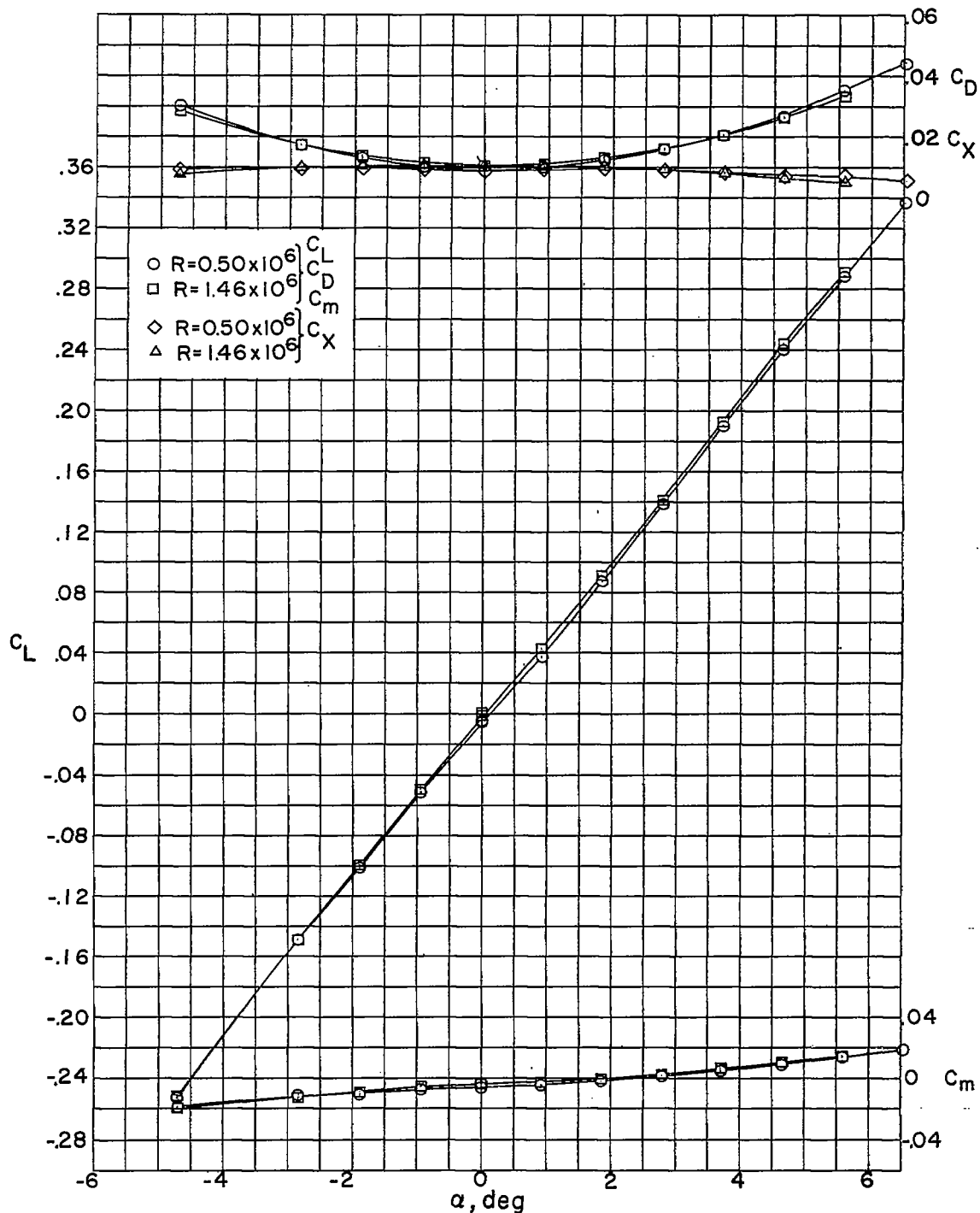


Figure 8.- Aerodynamic characteristics of the wing in the presence of the body for triangular wing 3 ( $\epsilon = 30^\circ$ ). Flagged symbols denote check values.

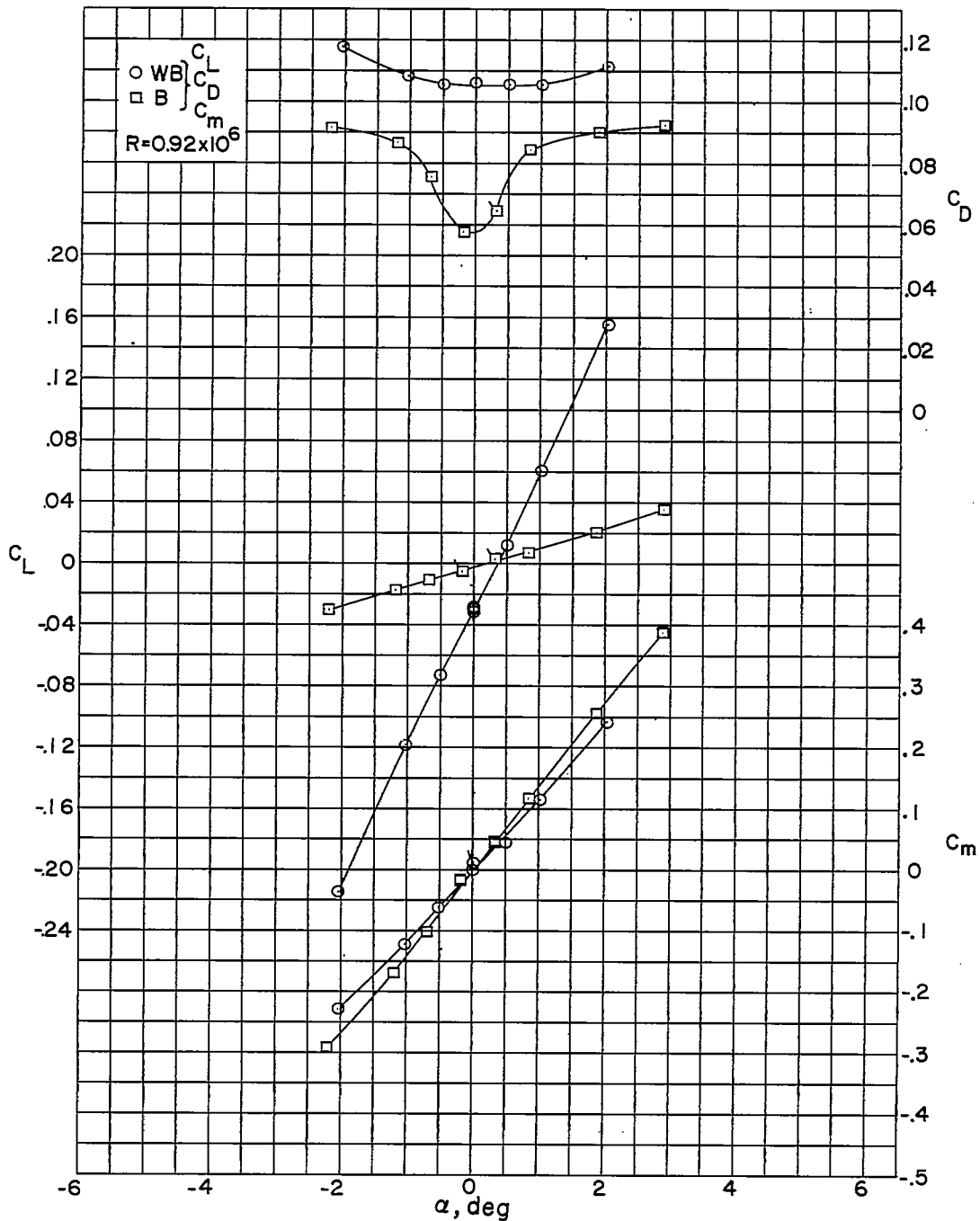


Figure 9.- Aerodynamic characteristics of the wing and body combination for triangular wing 4 ( $\epsilon = 30^\circ$ ) and the body alone. (Body-alone results are based on exposed area of triangular wing 4.) Flagged symbols denote check values.

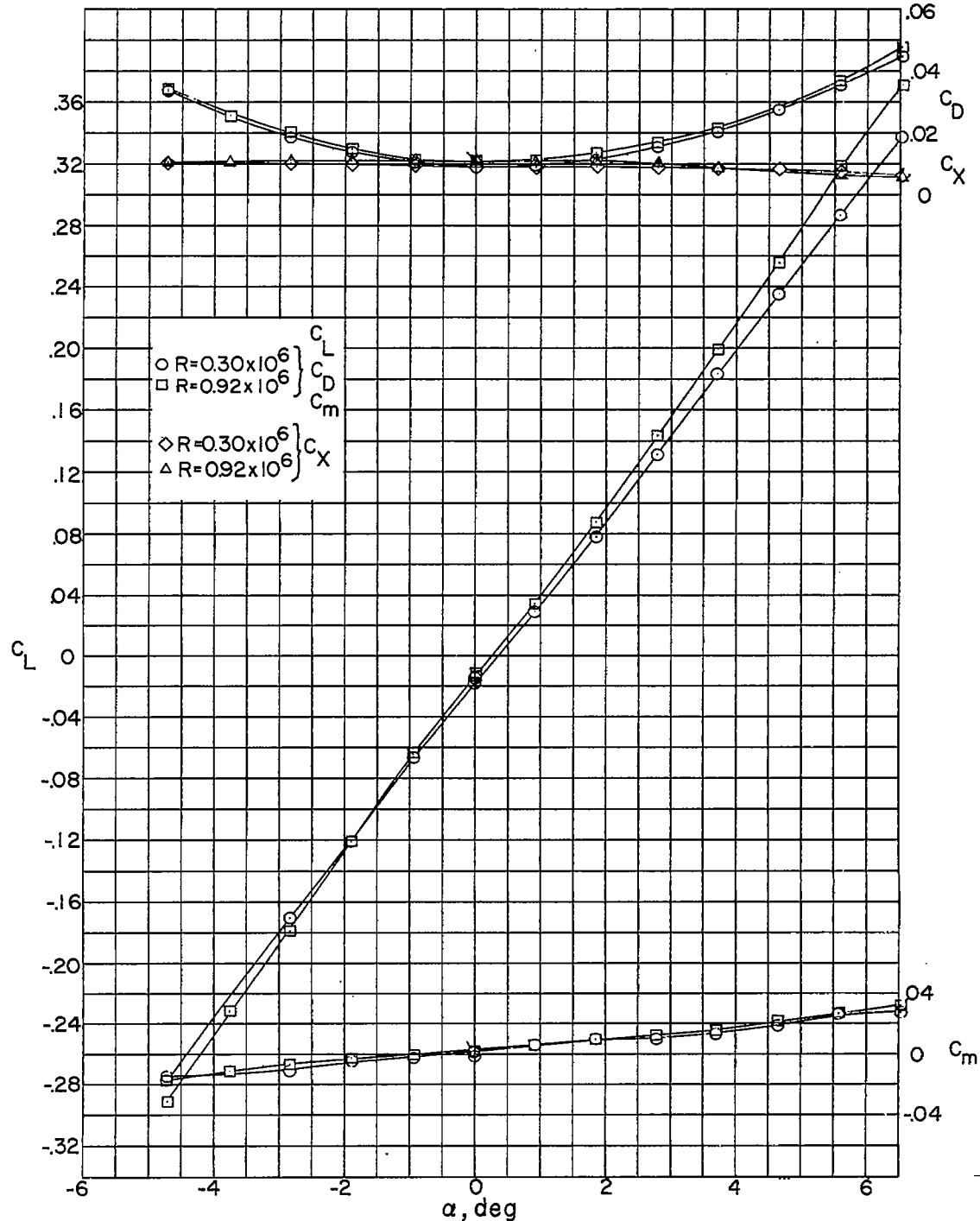


Figure 10.- Aerodynamic characteristics of the wing in the presence of the body for triangular wing 4 ( $\epsilon = 30^\circ$ ). Flagged symbols denote check values.

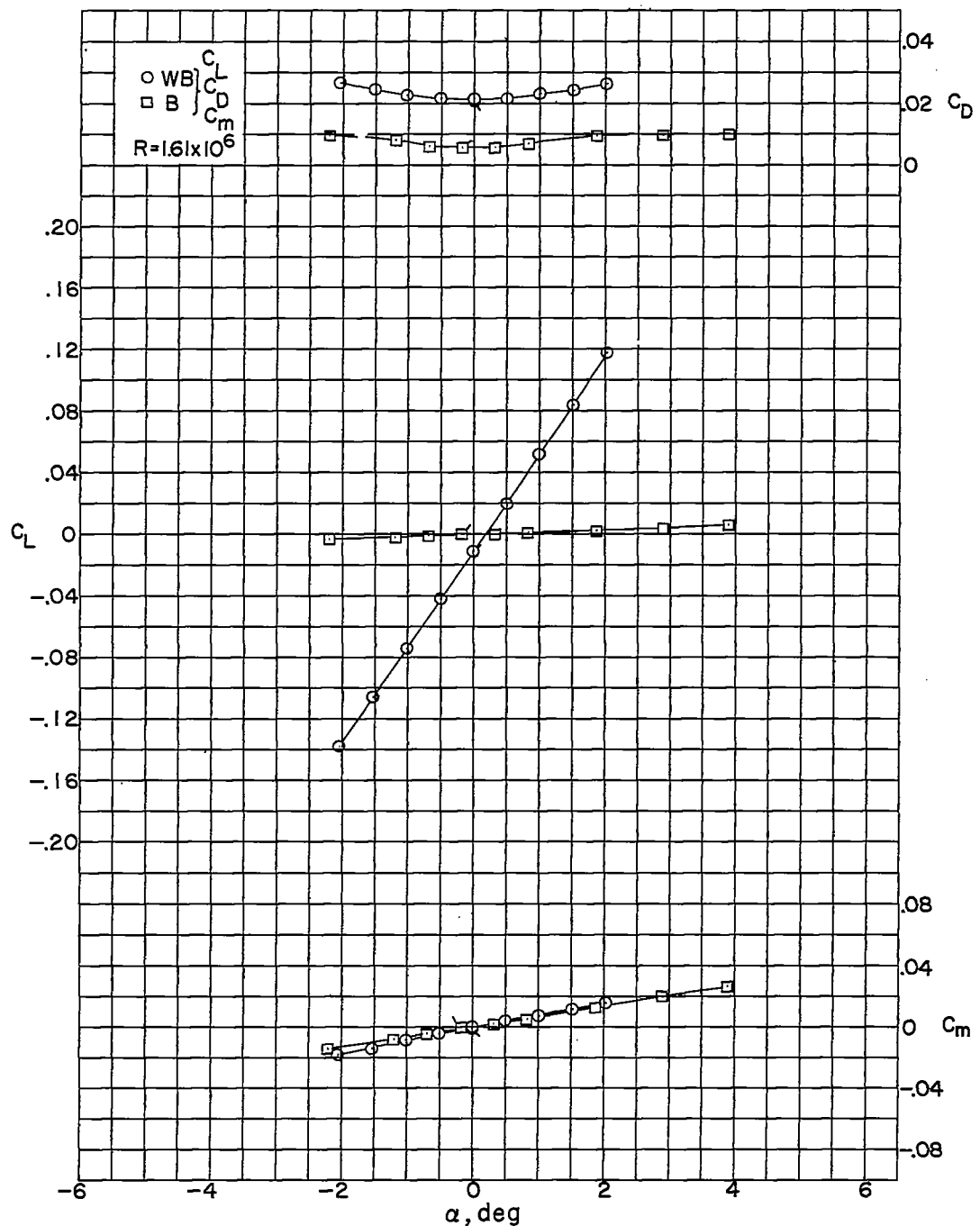


Figure 11.- Aerodynamic characteristics of the wing and body combination for triangular wing 5 ( $\epsilon = 45^\circ$ ) and the body alone. (Body-alone results are based on exposed area of triangular wing 5.) Flagged symbols denote check values.

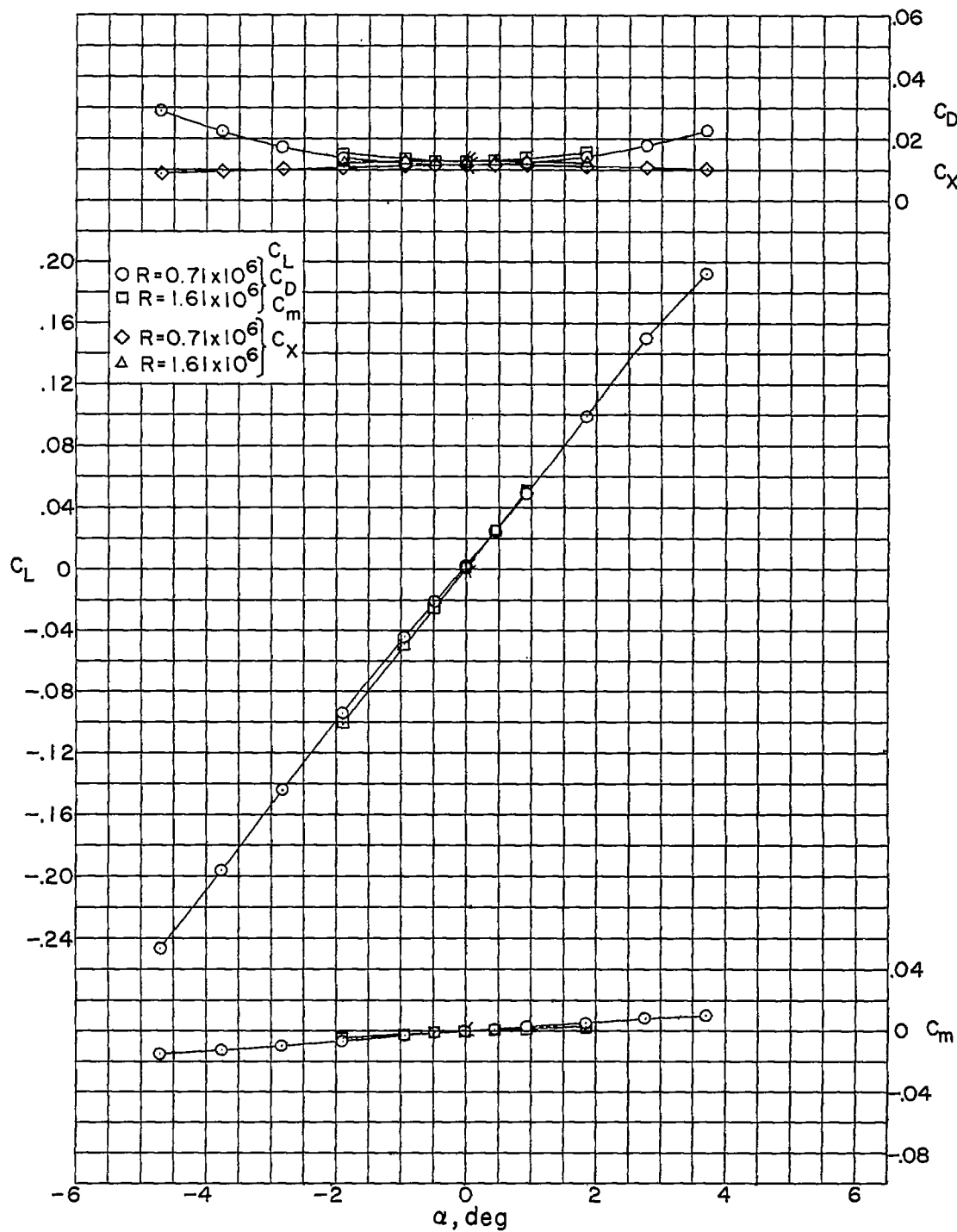


Figure 12.- Aerodynamic characteristics of the wing in the presence of the body for triangular wing 5 ( $\epsilon = 45^\circ$ ). Flagged symbols denote check values.

~~CONFIDENTIAL~~

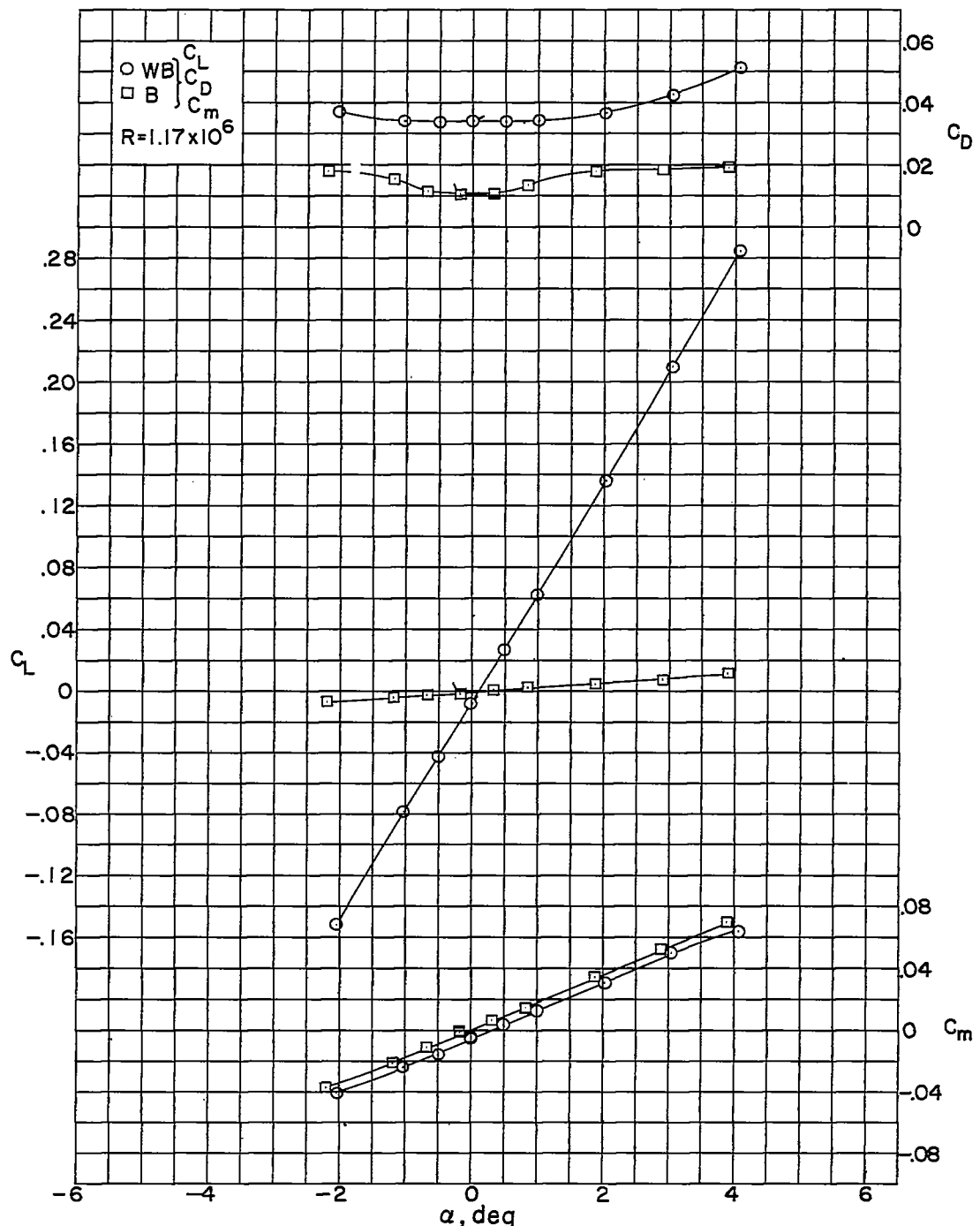


Figure 13.- Aerodynamic characteristics of the wing and body combination for triangular wing 6 ( $\epsilon = 45^\circ$ ) and the body alone. (Body-alone results are based on exposed area of triangular wing 6.) Flagged symbols denote check values.

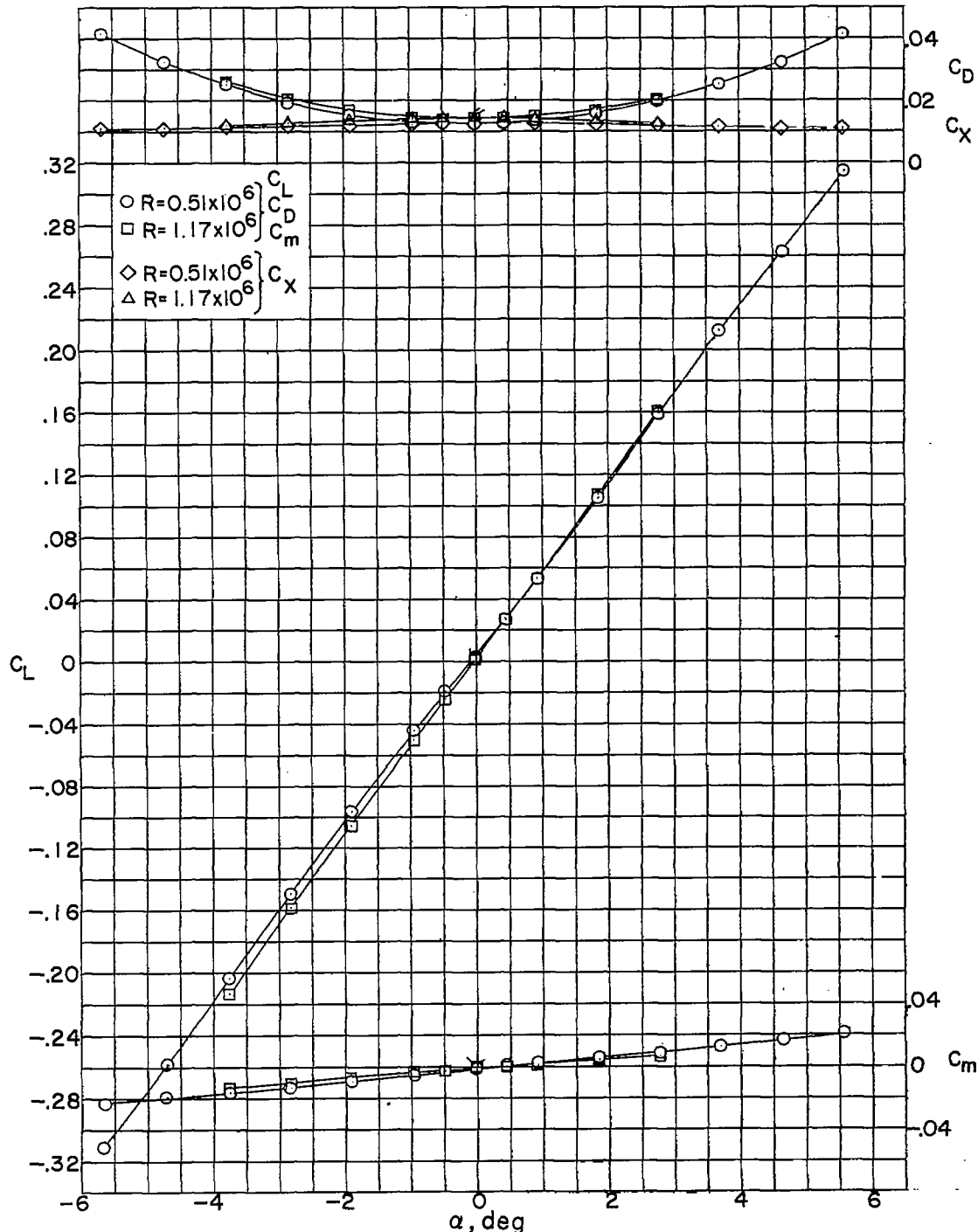


Figure 14.- Aerodynamic characteristics of the wing in the presence of the body for triangular wing 6 ( $\epsilon = 45^\circ$ ). Flagged symbols denote check values.

~~CONFIDENTIAL~~

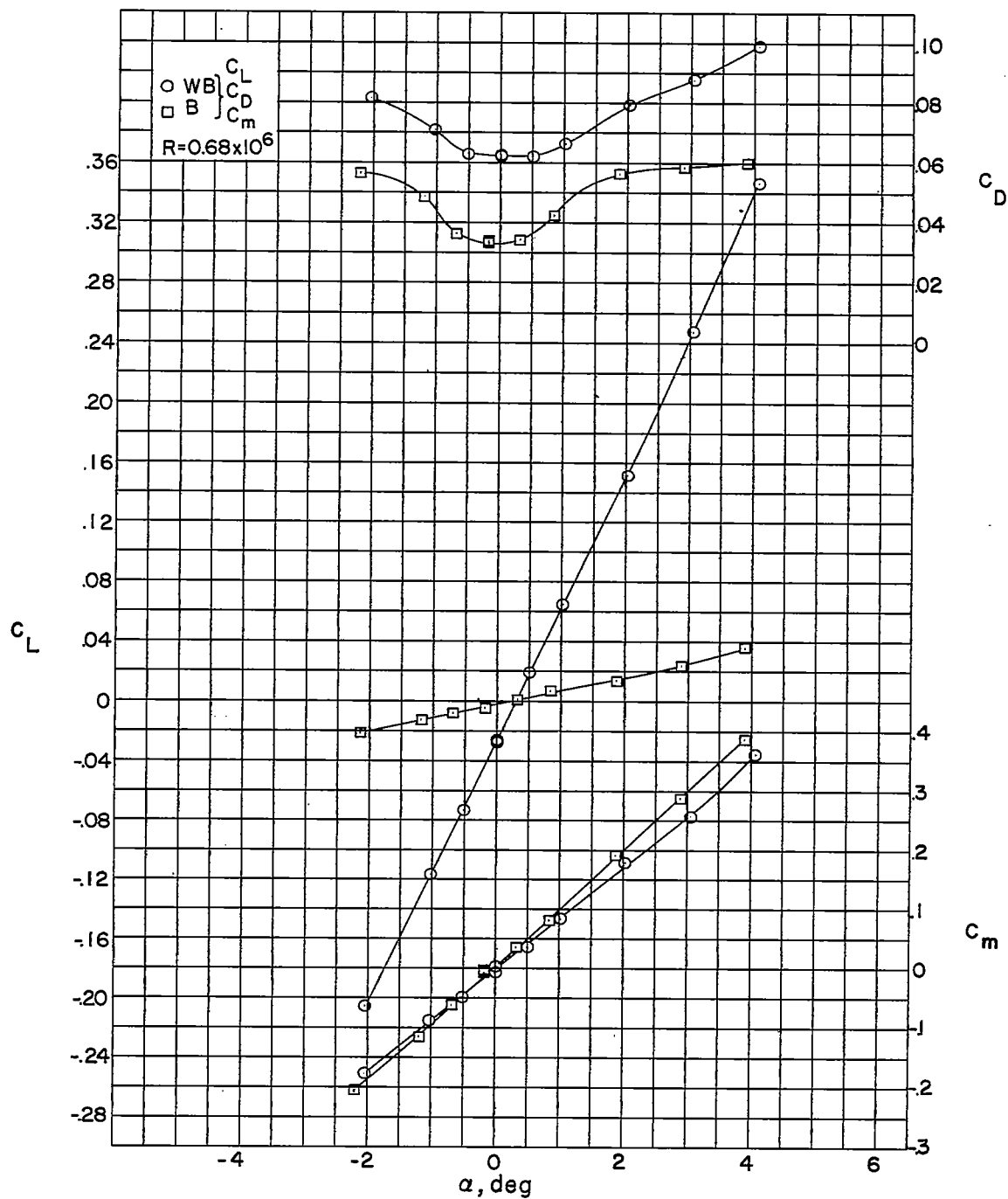


Figure 15.- Aerodynamic characteristics of the wing and body combination for triangular wing 7 ( $\epsilon = 45^\circ$ ) and the body alone. (Body-alone results are based on exposed area of triangular wing 7.) Flagged symbols denote check values.

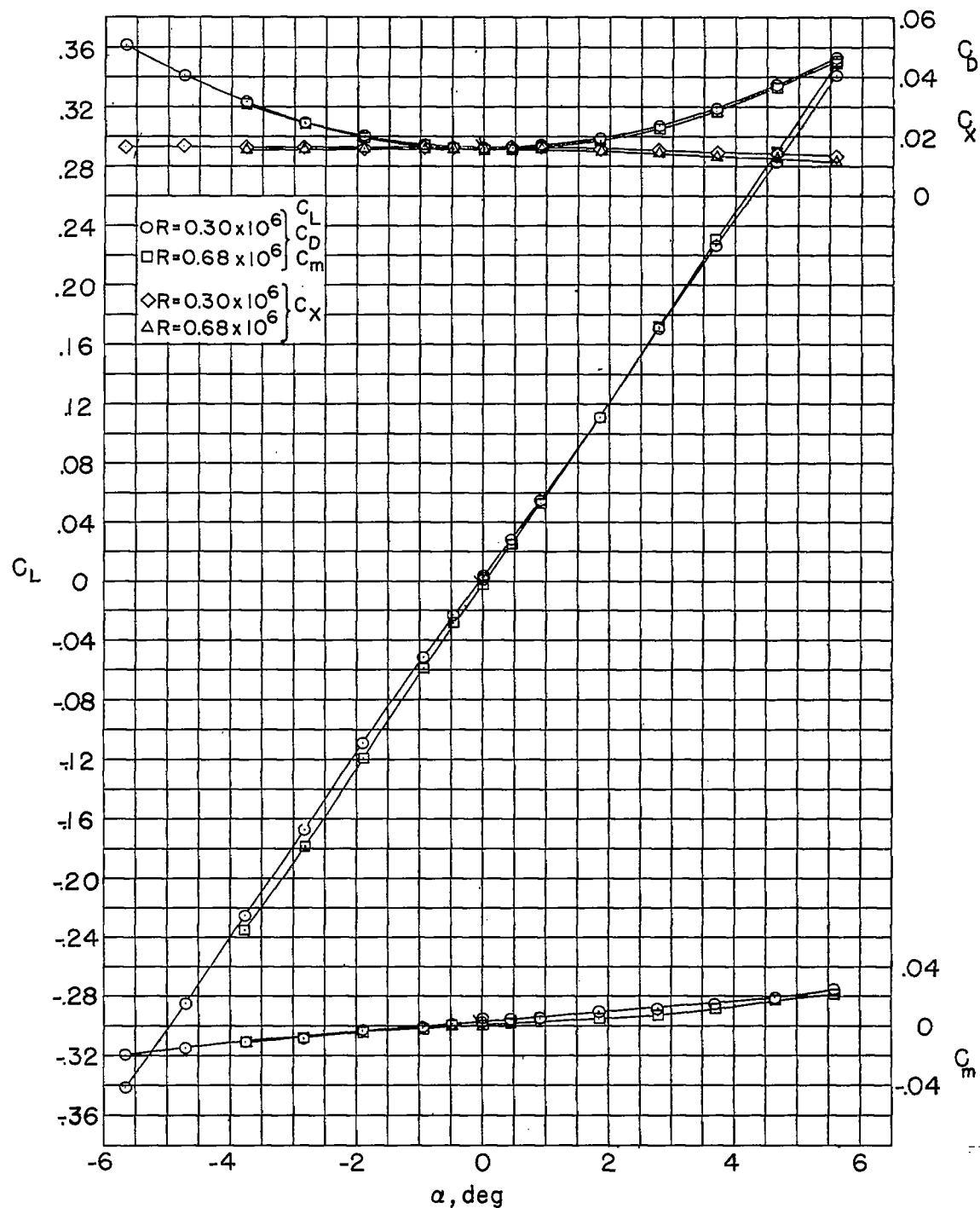


Figure 16.- Aerodynamic characteristics of the wing in the presence of the body for triangular wing 7 ( $\epsilon = 45^\circ$ ). Flagged symbols denote check values.

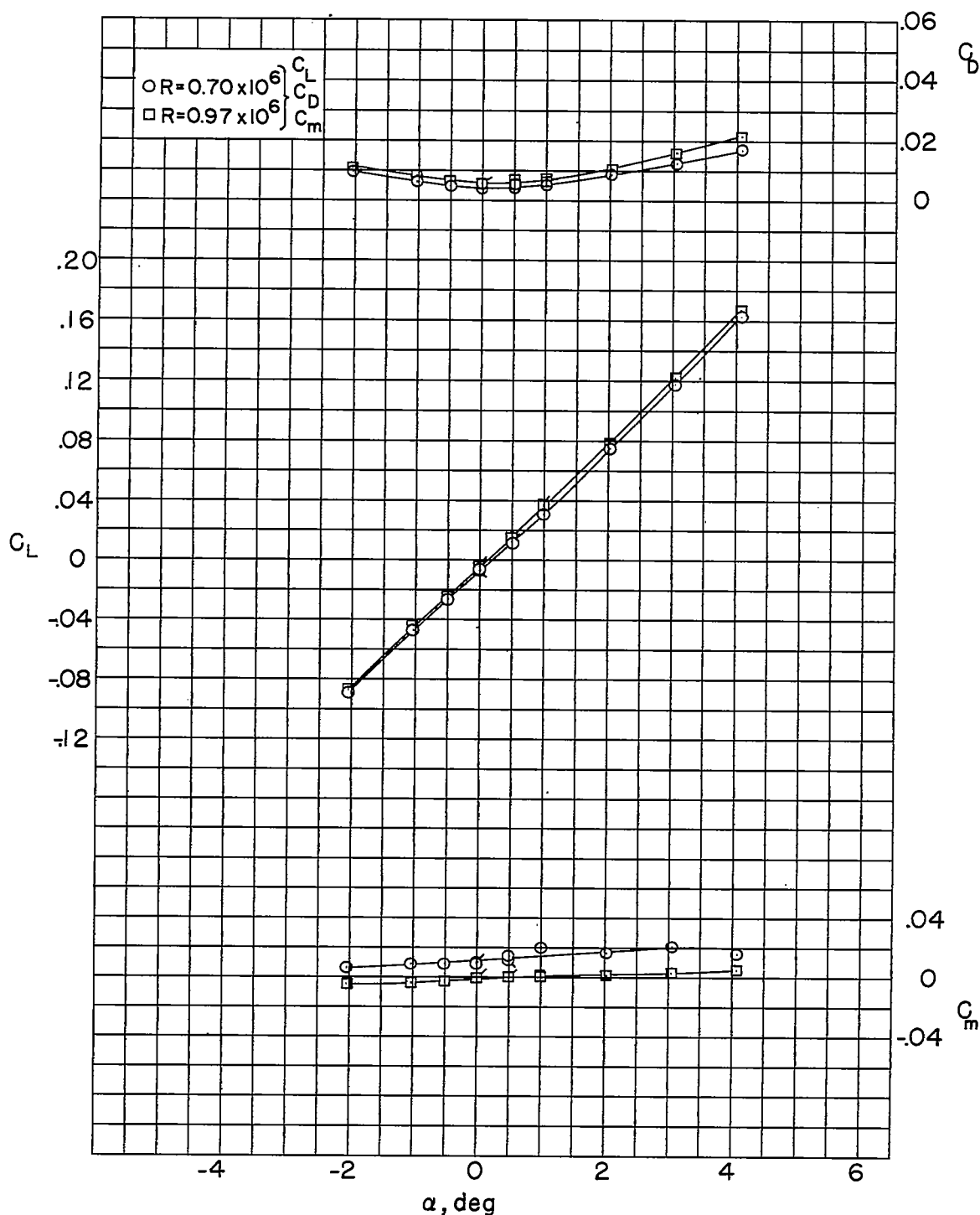


Figure 17.- Aerodynamic characteristics of triangular wing 2 ( $\epsilon = 30^\circ$ ) alone. Flagged symbols denote check values.

~~CONFIDENTIAL~~

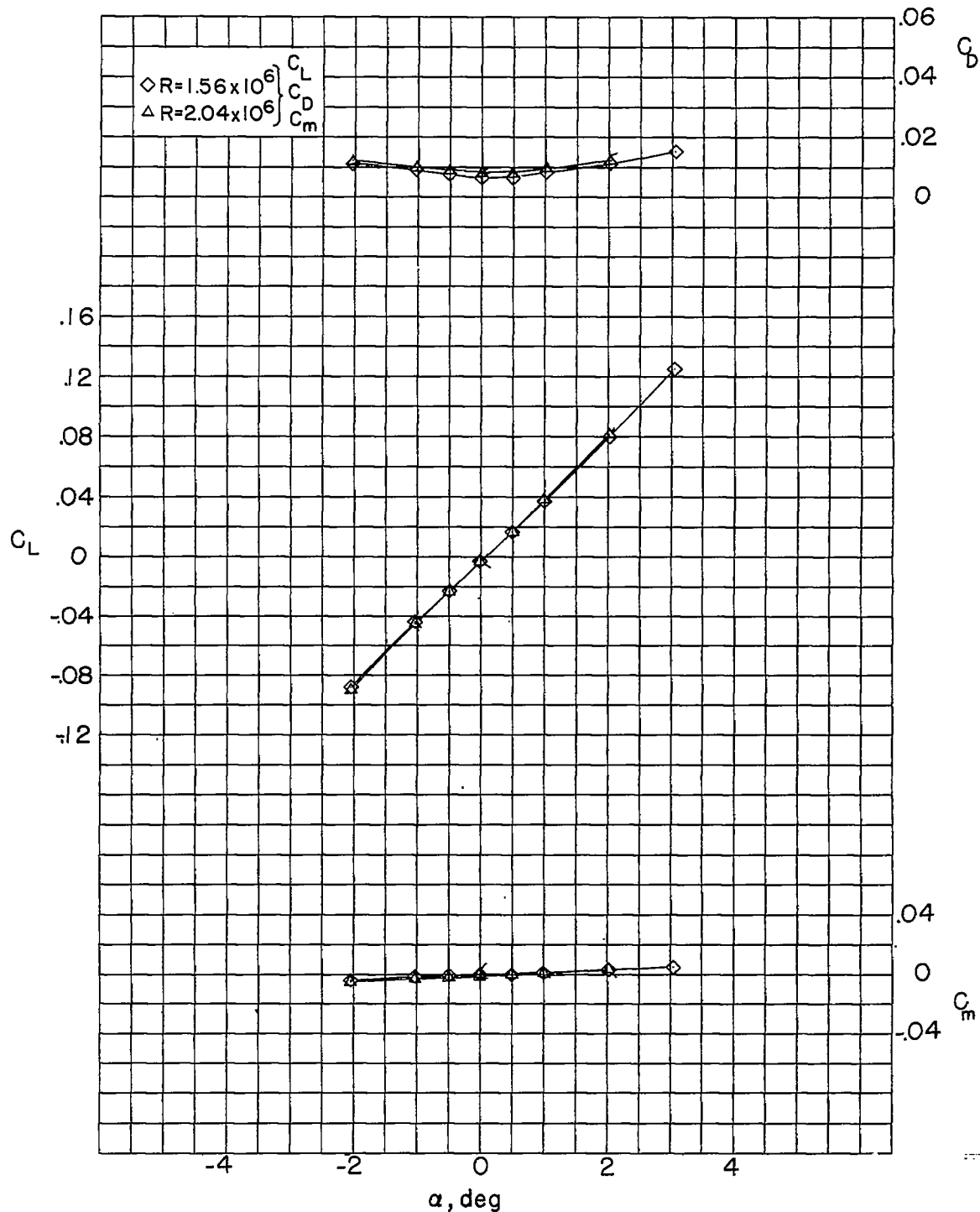


Figure 17.- Concluded.

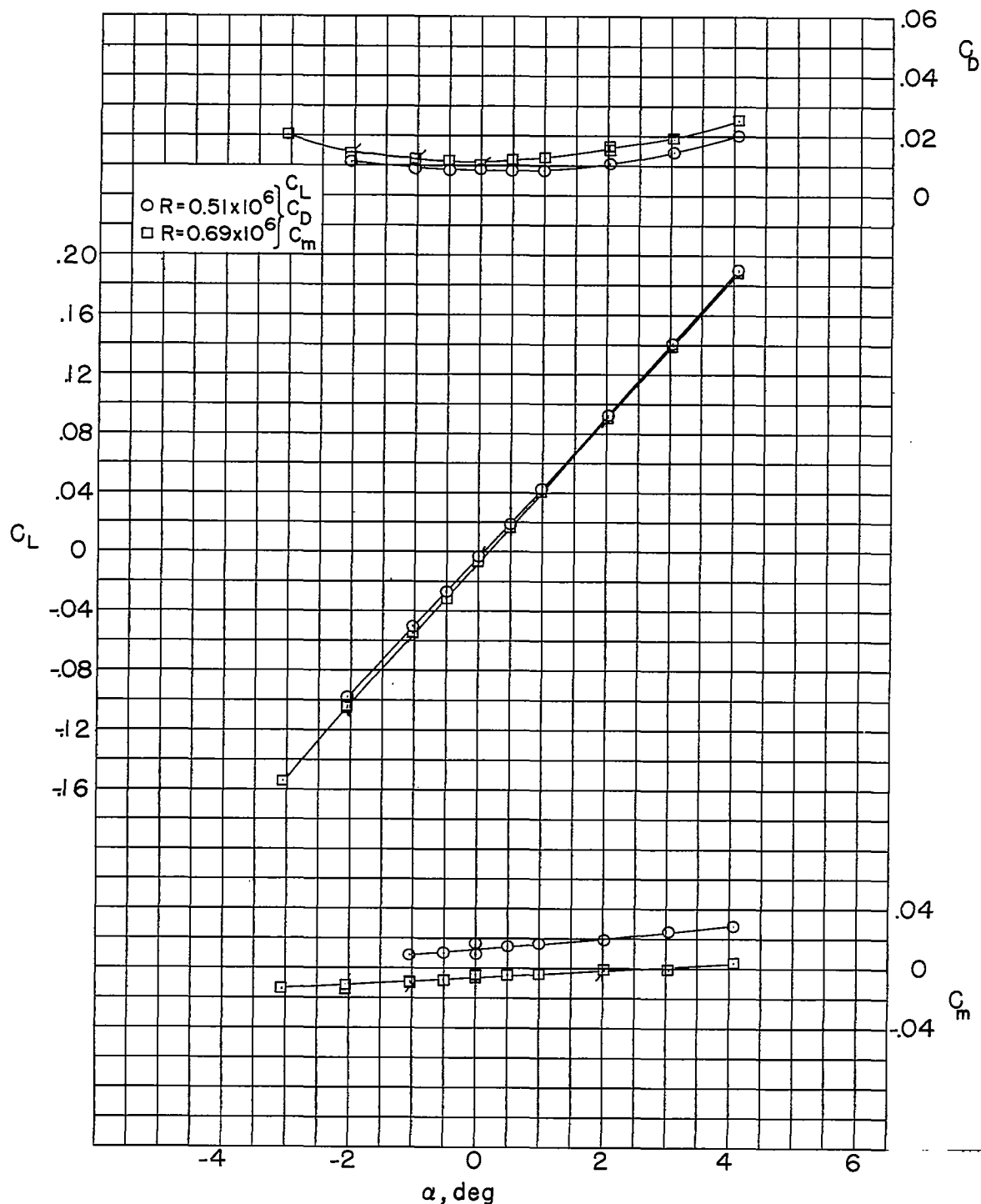


Figure 18.- Aerodynamic characteristics of triangular wing 6 ( $\epsilon = 45^\circ$ ) alone. Flagged symbols denote check values.

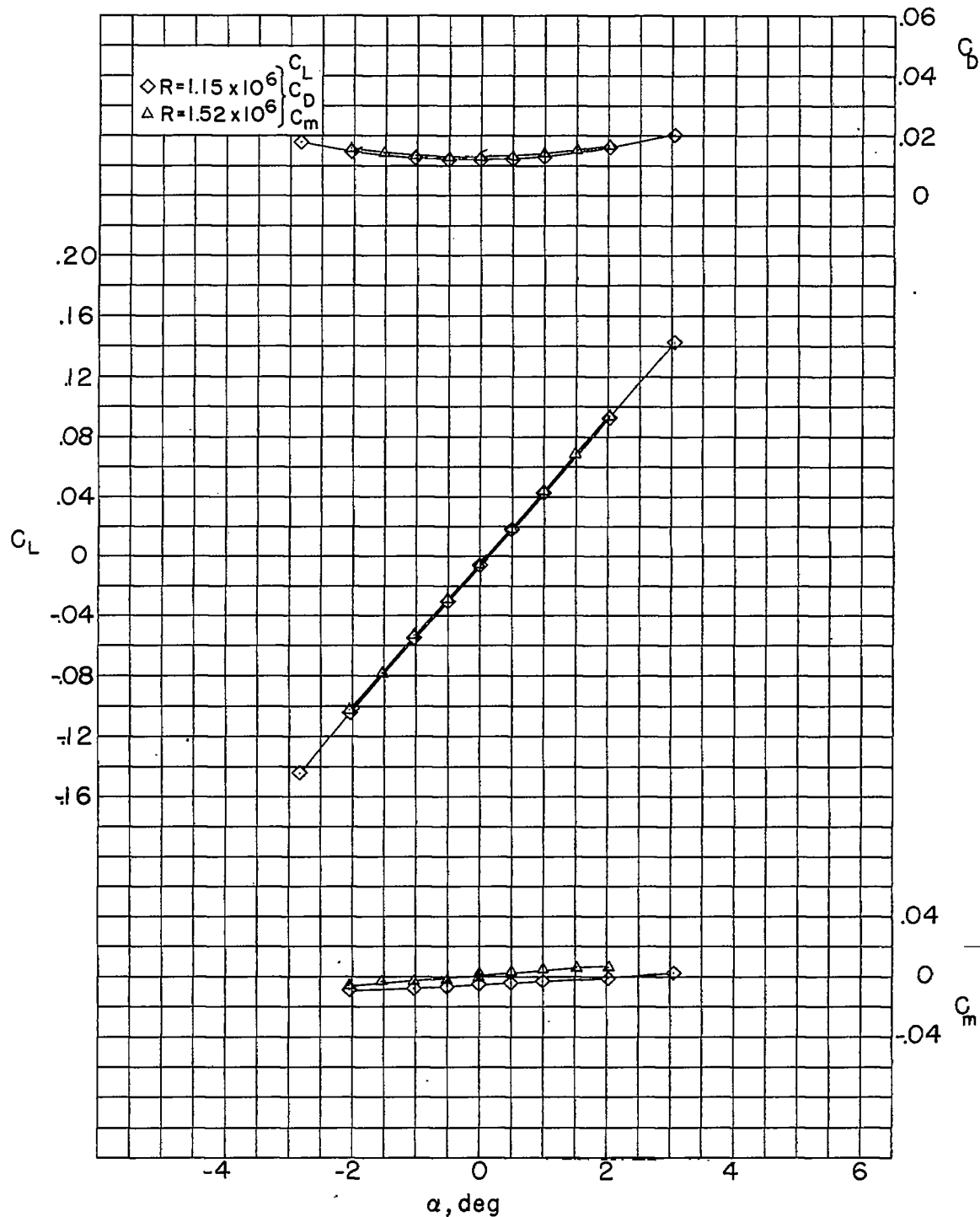


Figure 18.- Concluded.

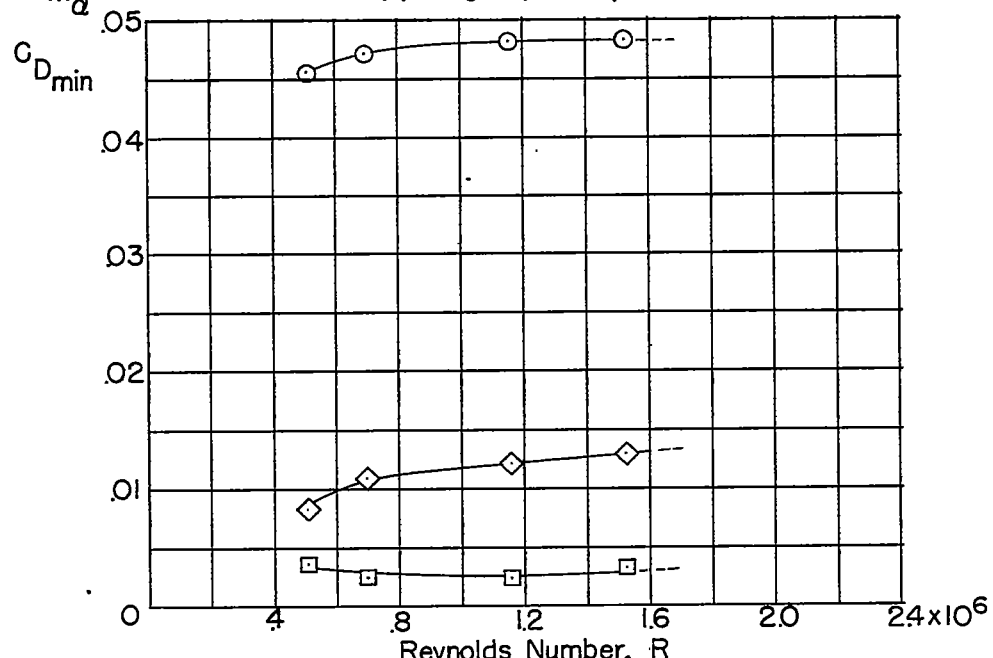
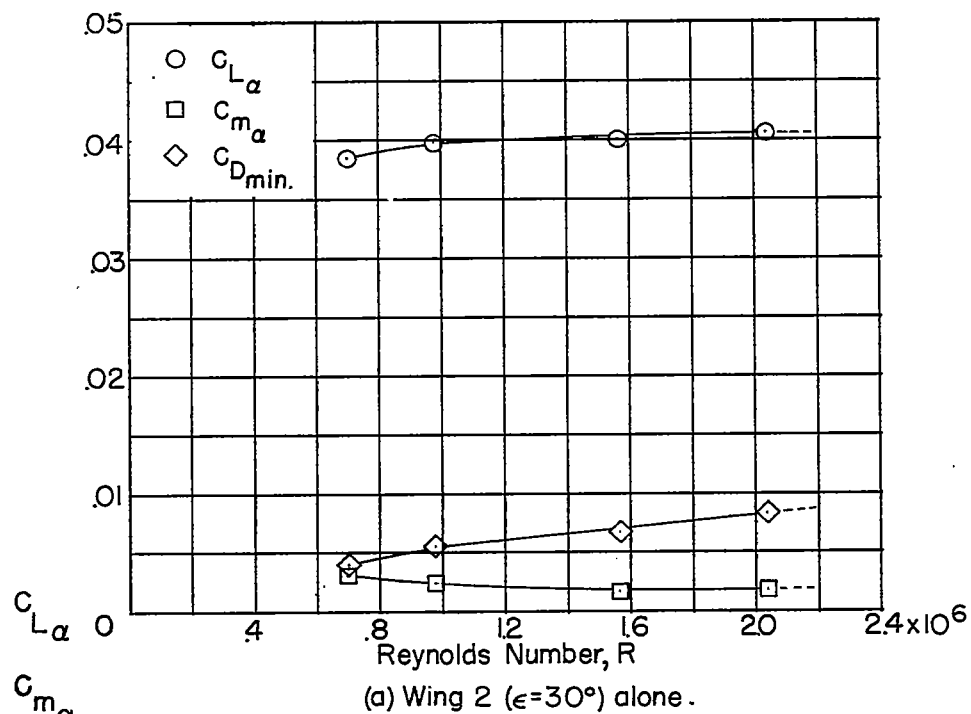
(b) Wing 6 ( $\epsilon = 45^\circ$ ) alone.

Figure 19.- Variation of the aerodynamic characteristics of wings 2 and 6 alone as a function of Reynolds number at  $M = 1.62$ .

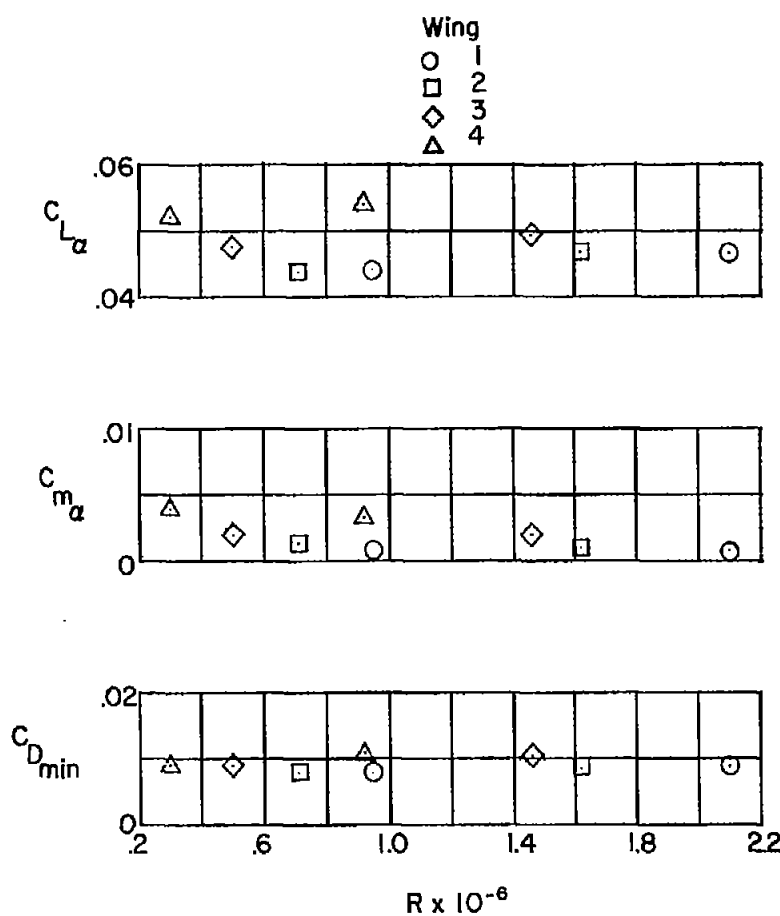
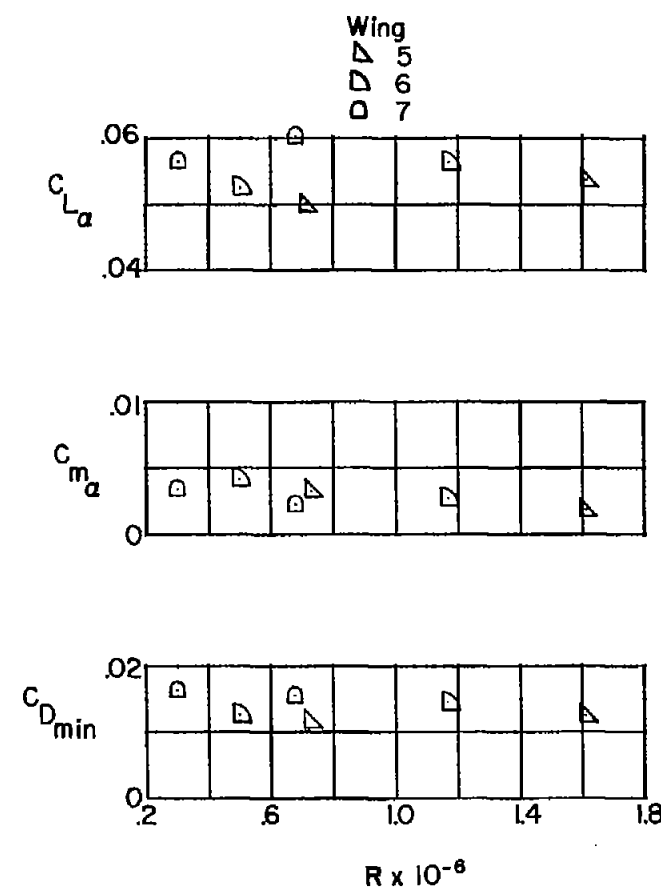
(a)  $\epsilon = 30^\circ$ .(b)  $\epsilon = 45^\circ$ .

Figure 20.- Effect of Reynolds number on the aerodynamic characteristics of the wing in the presence of the body, W(B).

Configuration	Experiment	Theory
WB	○	— Ref. 5
W(B)	□	— Ref. 5
B	△	- - - Ref. 9
W	◊	- - - Ref. 8

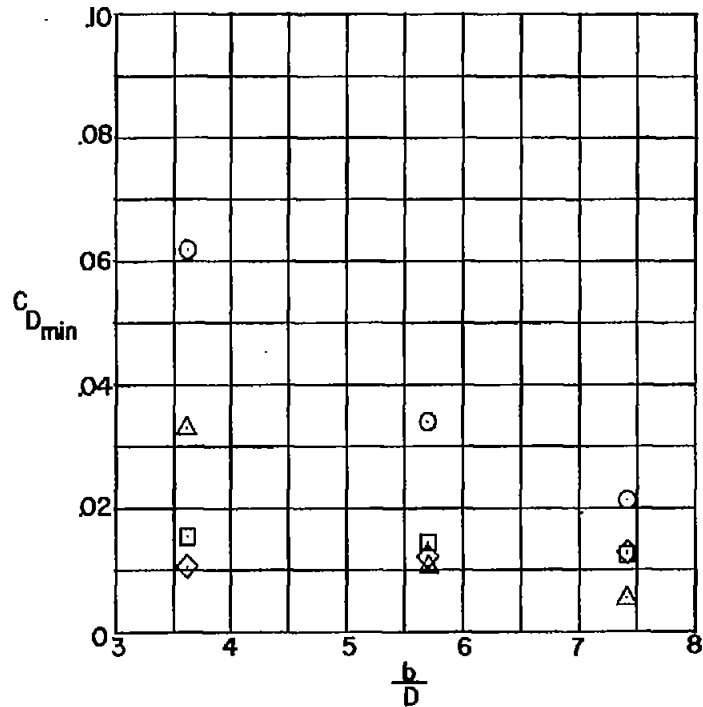
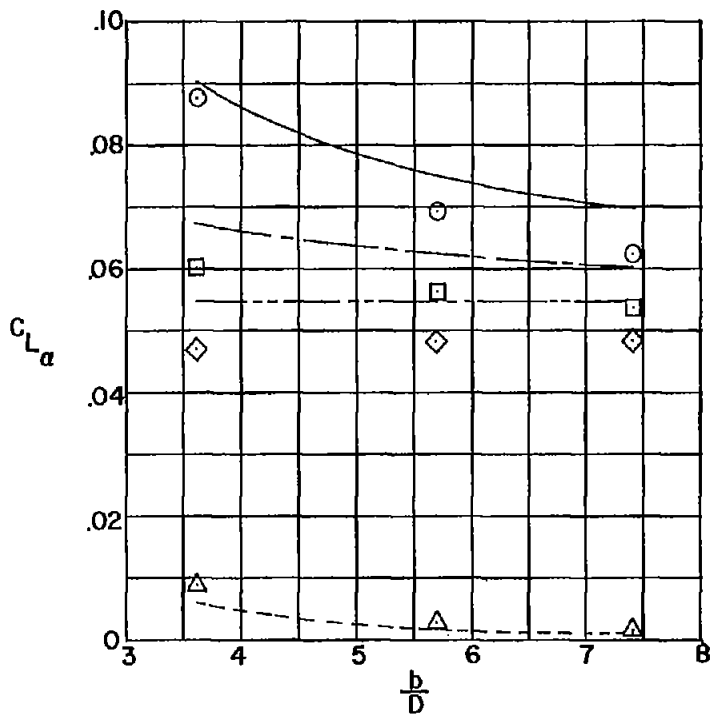


Figure 21.- Comparison between the experimental and theoretical aerodynamic characteristics of WB, W(B), W, and B for an  $n = 10.27$  body and a series of  $\epsilon = 30^\circ$  triangular wings at  $M = 1.62$ . Wing-alone values are obtained at equivalent Reynolds numbers.

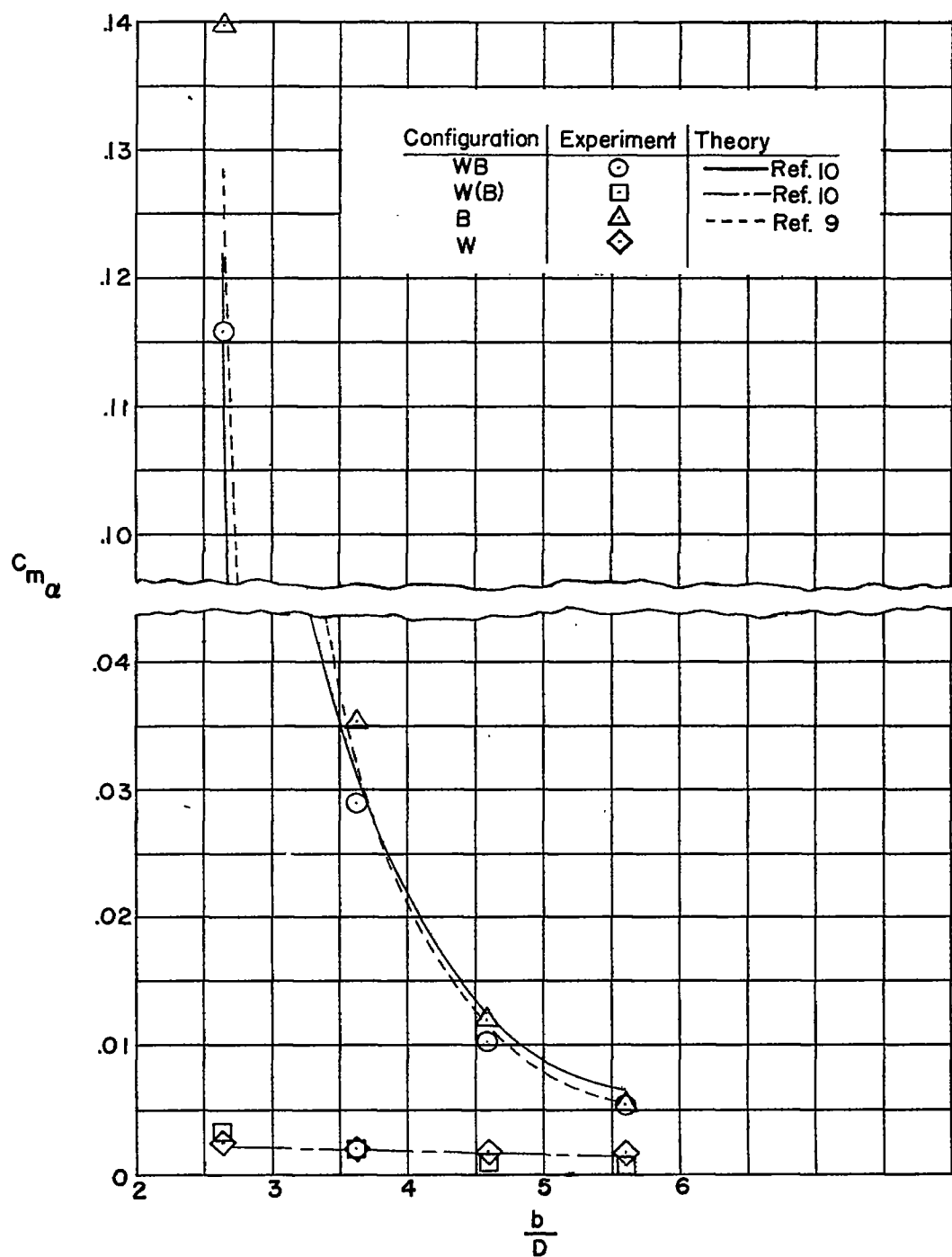


Figure 21.- Concluded.

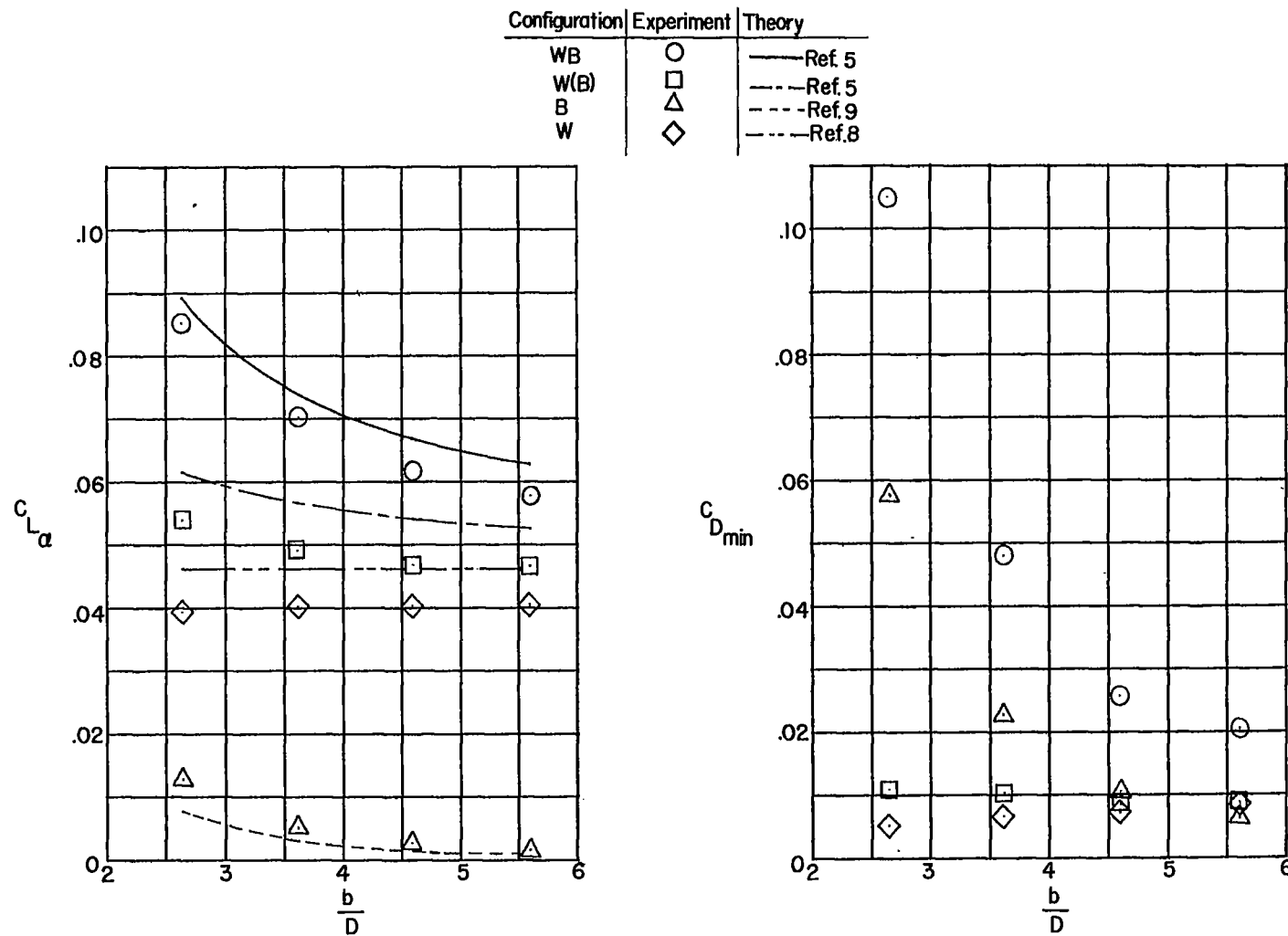


Figure 22.- Comparison between the experimental and theoretical aerodynamic characteristics of WB, W(B), W, and B for an  $n = 10.27$  body and a series of  $\epsilon = 45^\circ$  triangular wings at  $M = 1.62$ . Wing-alone values are obtained at equivalent Reynolds numbers.

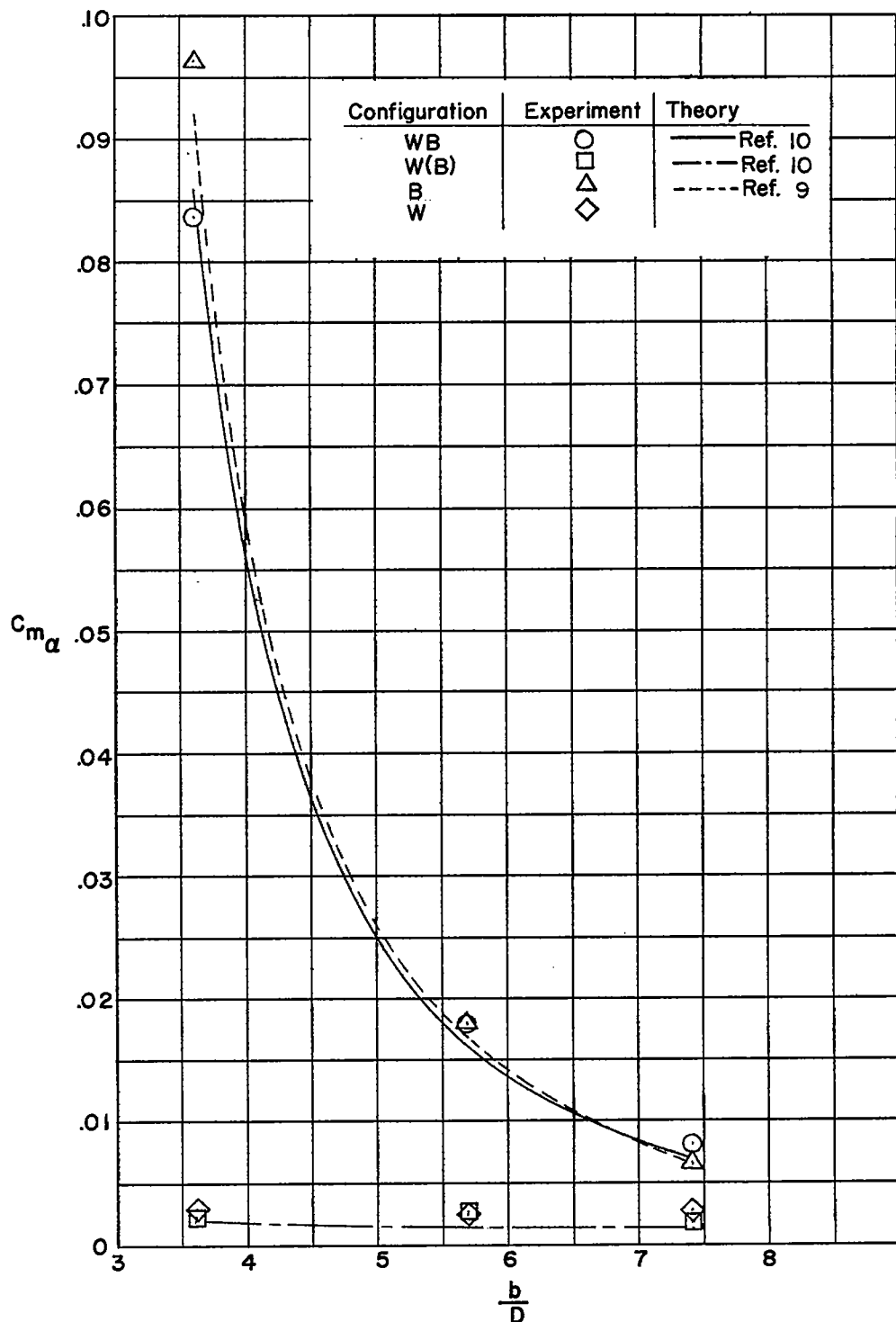
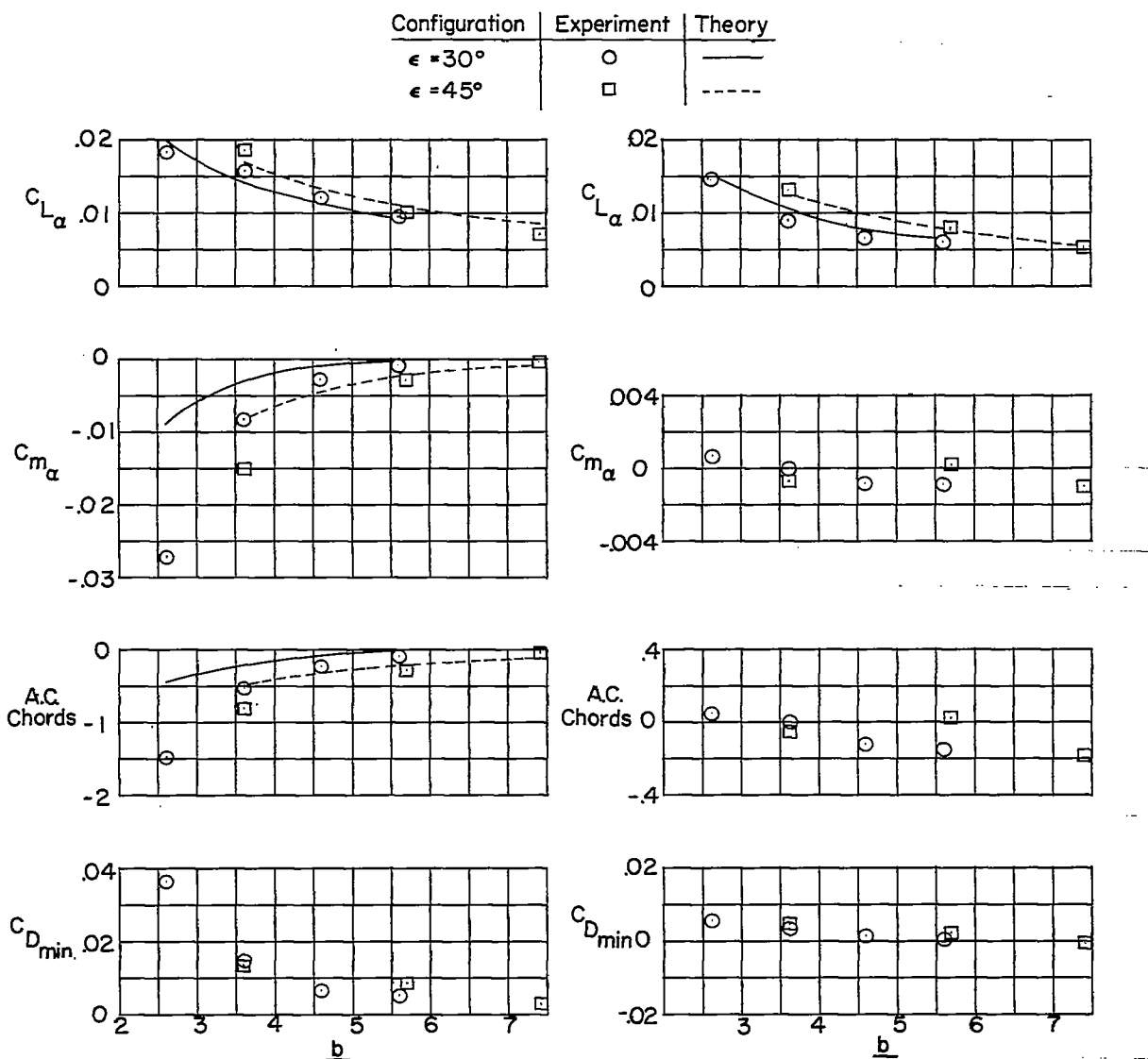
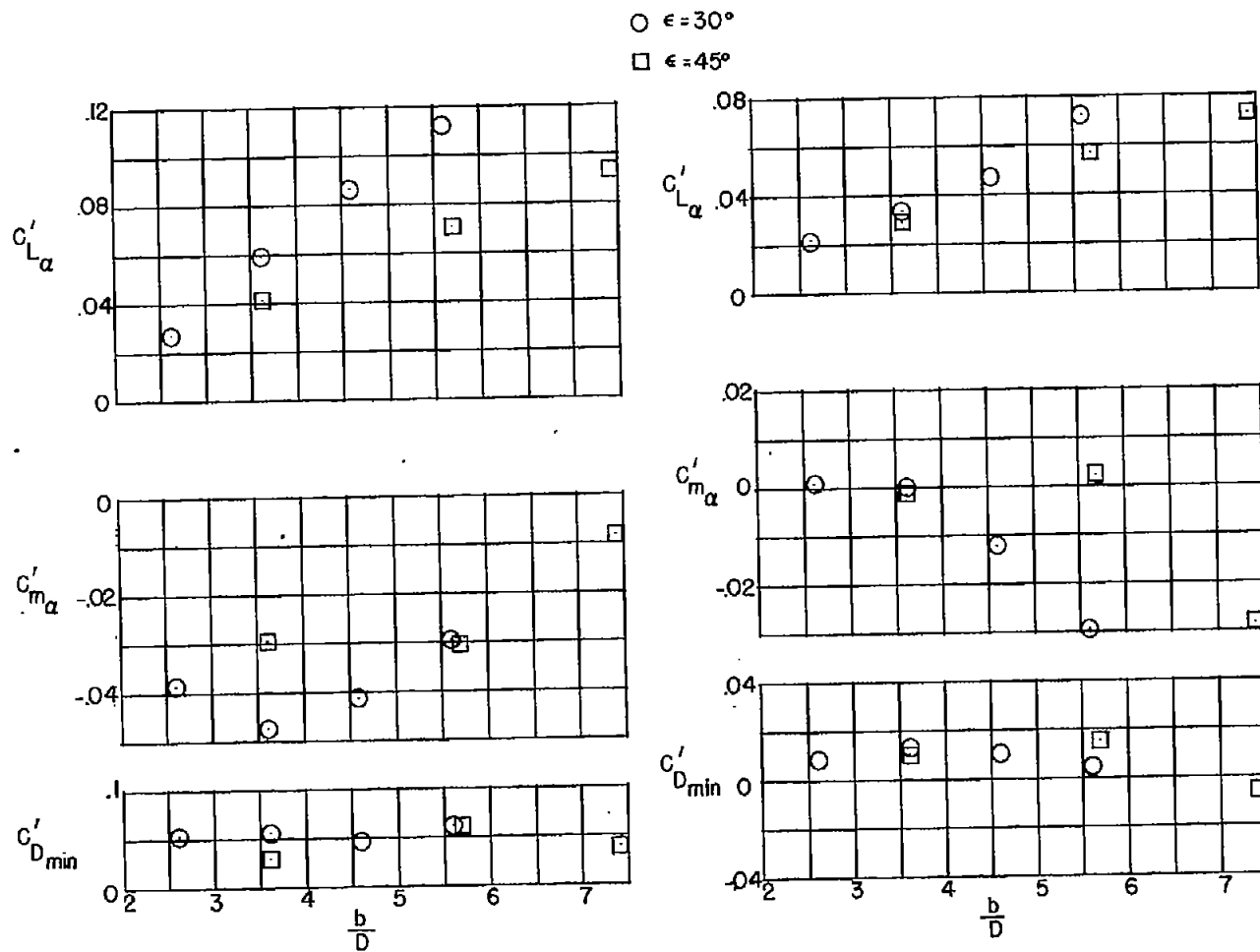


Figure 22.- Concluded.

(a)  $b(w)$ . Based on exposed wing area.(b)  $w(b)$ . Based on exposed wing area.Figure 23.- Interference quantities as a function of  $b/D$  for  $b(w)$  and  $w(b)$ .



(c)  $b(w)$ . Based on maximum body frontal area and maximum body diameter.

(d)  $w(b)$ . Based on maximum body frontal area and maximum body diameter.

Figure 23.- Concluded.

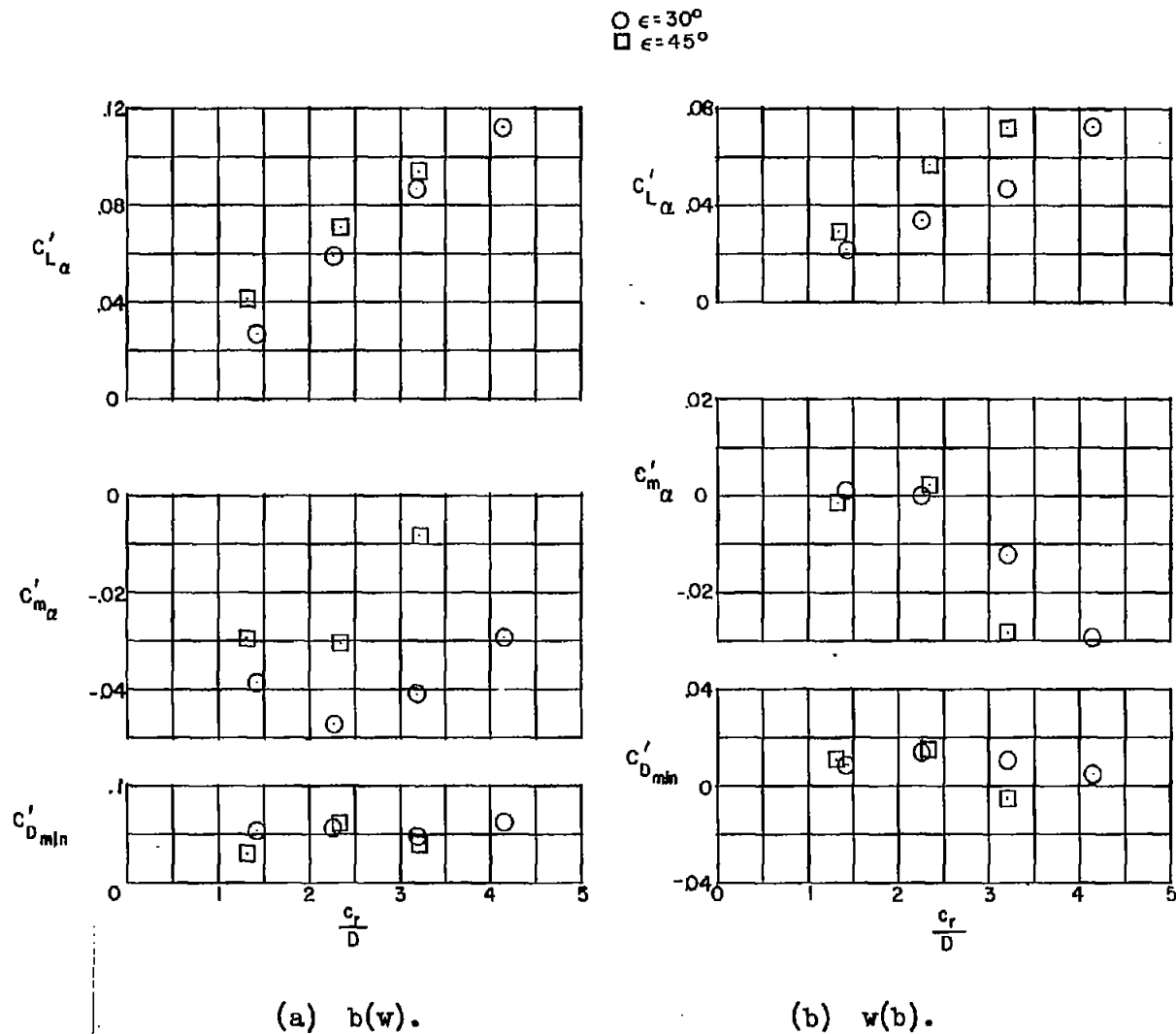


Figure 24.- Interference quantities as a function of  $c_r/D$  for  $b(w)$  and  $w(b)$ . Based on maximum body frontal area and maximum body diameter.

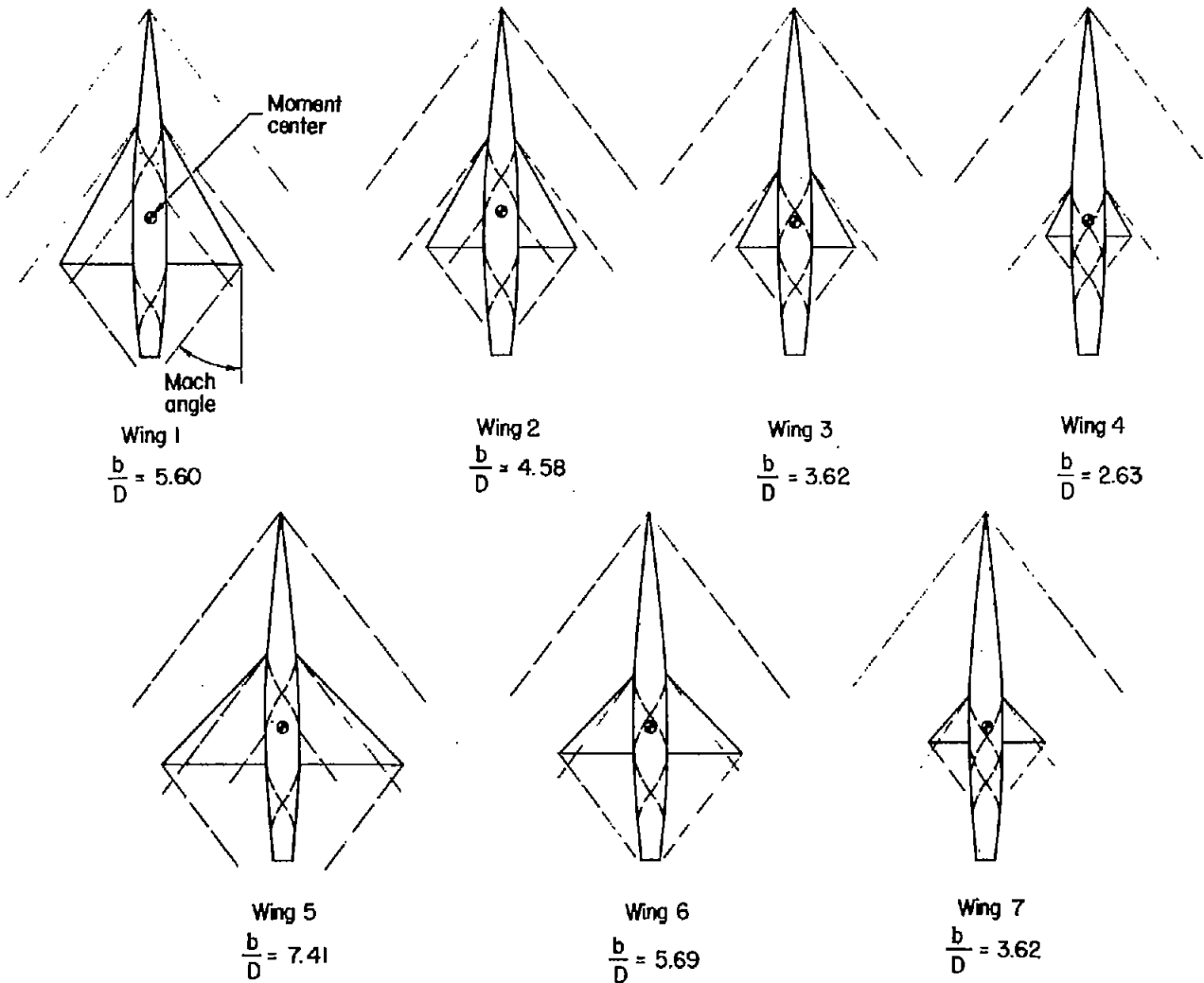


Figure 25.- Approximate location of nose shocks and Mach lines on the series of triangular wing and body combinations at  $M = 1.62$ .

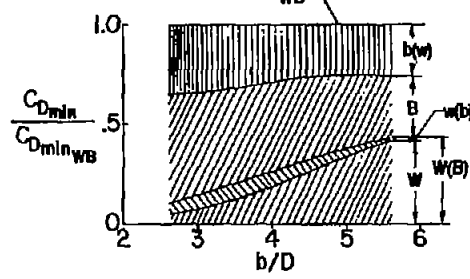
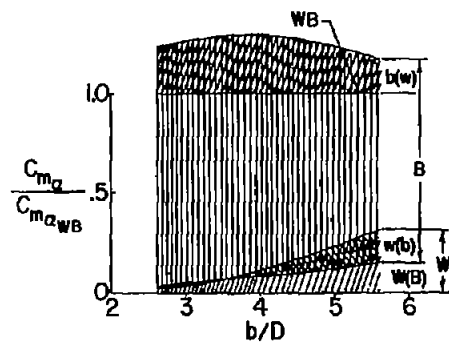
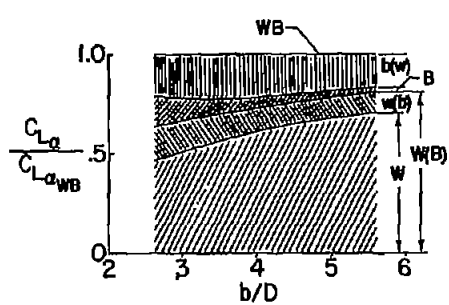
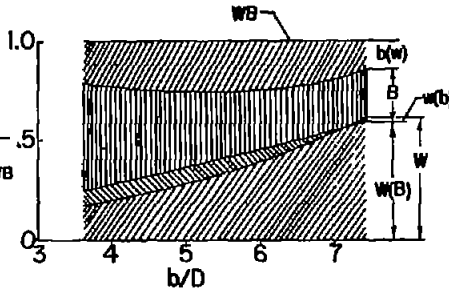
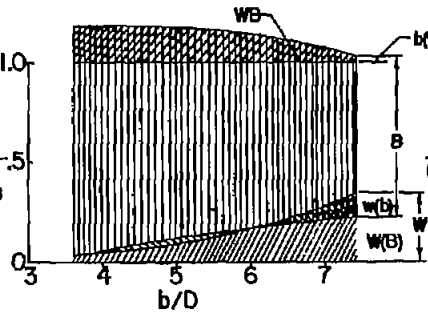
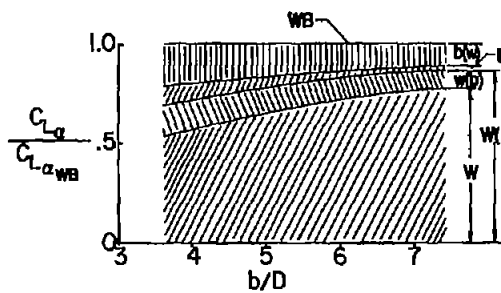
(a)  $\epsilon = 30^\circ$ .(b)  $\epsilon = 45^\circ$ .

Figure 26.- Incremental and interference quantities.